

FIGURE 4. Photopic ERGs recorded from 6- and 12-week-old rhodopsin P347L Tg rabbits. **(A)** Photopic ERGs elicited by five different stimulus intensities. **(B)** Photopic ERG mean amplitude versus flash intensity for the a- and b-waves in the TES-treated (○) and sham-stimulated (■) retinas. Average ratio (TES/sham) of the a- **(C)** and b-wave **(D)** amplitudes at 12 weeks of age ($n = 5$, each, mean \pm SEM). Pointwise comparison indicated a significant difference in a-wave amplitudes at 0.95 to 1.95 log cd·s/m² (Student's *t*-tests for two groups; * $P < 0.05$, ** $P < 0.01$), and in b-wave amplitudes at 1.48 and 1.95 log cd·s/m² (Student's *t*-tests for two groups; * $P < 0.05$, ** $P < 0.01$).

Effect of TES on Electroretinograms of Tg Rabbits

To evaluate the electrical properties of the rod and cone systems of rabbits, we recorded full-field scotopic and photopic ERGs. The scotopic ERGs elicited by different stimulus intensities from 6- and 12-week-old Tg rabbits are shown in Figure 3A. The amplitudes of the scotopic ERGs recorded from the eyes of 12-week-old Tg rabbits were not reduced compared with those from the eyes of 6-week-old Tg rabbits. The intensity-response curves for the a- and b-waves are plotted in Figure 3B. Scotopic ERG a-wave amplitudes of TES-treated eyes were not significantly different from those of sham-stimulated eyes. However, the b-wave amplitudes of the TES-treated eyes were slightly but significantly larger than those of the sham-stimulated eyes at the higher stimulus intensities.

We plotted the ratio (TES/sham-stimulated eye) of the amplitudes of the a- and b-waves for all intensities and performed statistical analyses on the differences (Figs. 3C, 3D). The differences in the ratios of the a-waves were not significant for all intensities. On the other hand, the ratios of the b-wave amplitudes were significantly larger at stimulus intensities higher than 0.95 log cd·s/m² (*P* < 0.05) in the TES-treated eyes.

The photopic ERGs obtained from Tg rabbits at 6 and 12 weeks of age are also shown in Figure 4A. The amplitudes of the TES-treated and sham-stimulated eyes at 12 weeks of age were slightly reduced compared with the ERGs recorded from 6-week-old Tg rabbits but the differences were not significant. However, the responses in the eye treated with TES were larger than those treated with sham stimulation (Fig. 4A).

The intensity-response curve for the a- and b-waves are plotted in Figure 4B. We also plotted the average ratio of TES-treated to sham-stimulated eyes at all intensities (Figs. 4C, 4D). For a-waves, there were significant differences between TES-treated and sham-stimulated eyes at 0.95 to 1.95 log cd·s/m² (*P* < 0.05, respectively). For b-waves, there were significant differences between them at 1.48 and 1.95 log cds/m² (*P* < 0.05).

Immunohistochemistry

Immunostaining with an antirhodopsin antibody and PNA lectin showed that the intensities of the immunostaining for both antirhodopsin antibody and PNA were stronger in the TES-treated retina (Figs. 5A-C) than the sham-stimulated retina (Figs. 5D-F).

DISCUSSION

Our electrophysiological and histological analyses showed that TES led to the survival of photoreceptors in the visual streak, and it also led to the preservation of ERG responses at higher stimulus intensities in rhodopsin P347L Tg rabbits. Although the cause of the photoreceptor degeneration in Tg rabbits is different from that in RCS rats and the phototoxic-induced degeneration in rats,^{20,23,25-27} TES also had a neuroprotective effect on the photoreceptors in Tg rabbits. These findings indicate that TES might have a similar neuroprotective effect on photoreceptors whose degeneration has different causes.

In the histological analysis, only the photoreceptors in the visual streak were rescued by TES, and in the areas outside the visual streak, the number of photoreceptors in the TES-treated retina was not significantly different from that in sham-stimulated retina. In Tg rabbits, the loss of photoreceptors was maximum in the visual streak where the photoreceptor density is highest, and the loss of photoreceptors was not significantly different at other regions outside visual streak at 12 weeks of age.²⁰ Therefore, at 12 weeks of age, the loss of photoreceptors was striking only in the visual streak, indicating that the neuroprotection of photoreceptors was limited to the visual streak.

Immunohistochemical analysis showed that the intensity of both PNA and rhodopsin immunostainings was stronger in the TES-treated retinas than in the sham-stimulated retinas in the visual streak.

However, the results of ERGs indicated that TES preserved the cone components better than rod components, although in Tg rabbits the rod components are more affected than the cones.^{20,23} Although it was not determined why the cone components were better preserved than the rod components, one possibility is that TES promoted the survival of both rod and cone photoreceptors, and the rescued rods secreted a cone viability factor to rescue the cone photoreceptors.²⁸ Otherwise, at 12 weeks of age, photoreceptors near the visual streak were much more affected than those outside the visual streak,²⁰ therefore the differences of ERG amplitudes of full field ERGs between TES-treated and sham-stimulated retinas might be detected only at higher stimulus intensities.

There are some possible mechanisms for the neuroprotection of photoreceptors. First, TES increased the expression of the mRNA and protein levels of neurotrophic factors (e.g., insulin-like growth factor-1 (IGF-1), brain-derived neurotrophic

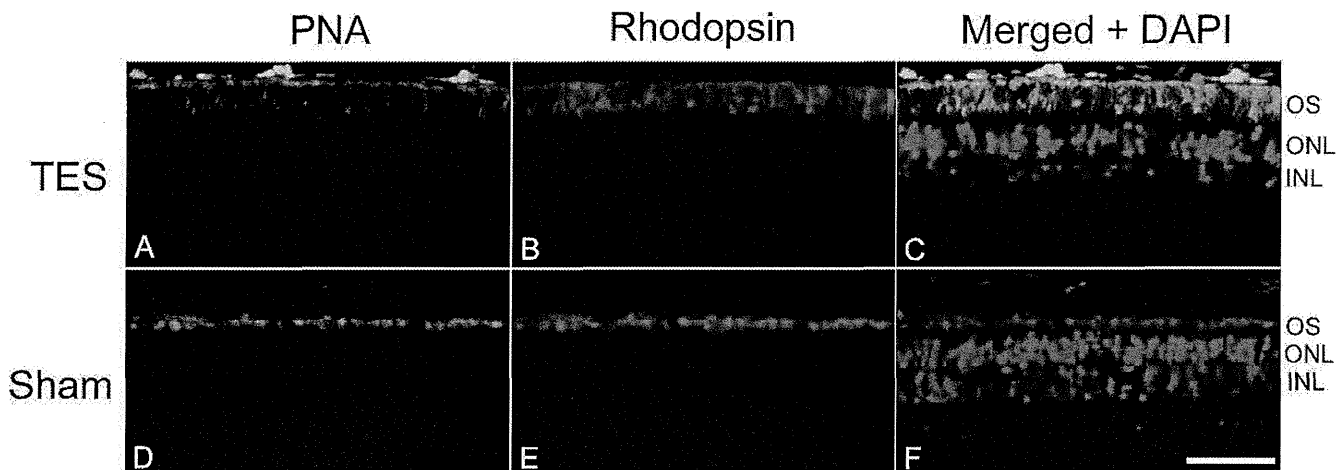


FIGURE 5. Immunohistochemical analysis of rod and cone photoreceptors triple labeled with rhodopsin (green), PNA (red), and DAPI (blue) in TES-treated (A-C) and sham-stimulated retinas (D-F) at 12 weeks of age (approximately 4 mm inferior to the optic nerve head). Intensities of rhodopsin and PNA immunostaining are stronger in the TES-treated ratio than in the sham-stimulated retina. Scale bar = 50 μm.

factor (BDNF), ciliary neurotrophic factor, or B-cell lymphoma-2 in the retinas after TES.^{11,17} A second possibility is that TES reduced the expression of the TNF super families and Bax, which are related to apoptosis signaling in retinal cells.²⁹ Cultured rat Müller cells exposed to electrical currents have been shown to express IGF-1, BDNF, and fibroblast growth factor-2 (FGF-2).³⁰⁻³² Other types of electrical stimulation to the retinas, such as subretinal electrical stimulation, increases the expression of FGF-2 in the retinas.³³ Unfortunately, we did not determine whether the expression of any of these neurotrophic factors was increased after TES in the Tg rabbit retinas.

Another possible mechanism for the TES-induced neuroprotection was an increase of chorioretinal blood circulation by TES.^{34,35} In clinical studies, TES has been shown to improve the visual function of patients with retinal artery occlusion.^{36,37} Thinning of the vascular plexus and the development of aberrant vessels have been reported in RP patients and animal models of RP.³⁸⁻⁴¹ This indicates that retinal blood circulation might be reduced in Tg rabbits. TES might have some neuroprotective effects on photoreceptors by increasing chorioretinal blood circulation.

We did not examine whether TES was neuroprotective for the photoreceptors in the peripheral retina. In Tg rabbits at the age of 48 weeks, almost all of the photoreceptors were lost^{20,27}; however, it takes a long time to investigate the neuroprotective effects of TES on the entire retina until the age of 48 weeks from 6 weeks, so it is difficult to continue the treatment until 48 weeks because weekly anesthesia and treatment put a heavy load on animals and is adverse to the animal welfare for long-term experiments. The results that TES did have neuroprotective effects on photoreceptors in the visual streak at 12 weeks of age were enough to lead us to determine the neuroprotection of TES on the photoreceptors in Tg rabbits.

Rhodopsin P347L Tg rabbits are an adRP model of human RP. Our results indicate that TES might have a neuroprotective effect on the photoreceptors in RP patients with the same mutation. Schatz et al.¹⁸ performed a prospective, randomized sham-controlled clinical study, and reported that TES improved the visual function in RP patients. From these neuroprotective effects of TES already published and our results, TES might exert a neuroprotective effect on photoreceptors of different animals with RP. Additional investigations on different animal models are necessary to determine which type of RP was the indication of TES treatment.

In conclusion, TES had a neuroprotective effect on the photoreceptors in the visual streak of rhodopsin P347L Tg rabbits, which is a model of human adRP. These results support and encourage clinical trials of TES for RP patients.

Acknowledgments

The authors thank Yuko Furukawa and Emi Higasa for technical assistance, and Duco I. Hamasaki for help with the manuscript.

References

- Marmor MF, Aguirre G, Arden G, et al. Retinitis pigmentosa: a symposium on terminology and methods of examination. *Ophthalmology*. 1983;90:126-131.
- Pagon RA. Retinitis pigmentosa. *Surv Ophthalmol*. 1988;33:137-177.
- Hartong DT, Berson EL, Dryja TP. Retinitis pigmentosa. *Lancet*. 2006;368:1795-1809.
- Berson EL, Rosner B, Sandberg MA, et al. A randomized trial of vitamin A and vitamin E supplementation for retinitis pigmentosa. *Arch Ophthalmol*. 1993;111:761-772.
- Sieving PA, Caruso RC, Tao W, et al. Ciliary neurotrophic factor (CNTF) for human retinal degeneration: phase I trial of CNTF delivered by encapsulated cell intraocular implants. *Proc Natl Acad Sci U S A*. 2006;103:3896-3901.
- Ali RR, Sarra GM, Stephens C, et al. Restoration of photoreceptor ultrastructure and function in retinal degeneration slow mice by gene therapy. *Nat Genet*. 2000;25:306-310.
- Bainbridge JW, Smith AJ, Barker SS, et al. Effect of gene therapy on visual function in Leber's congenital amaurosis. *N Engl J Med*. 2008;358:2231-2239.
- Zrenner E, Bartz-Schmidt KU, Benav H, et al. Subretinal electronic chips allow blind patients to read letters and combine them to words. *Proc Biol Sci*. 2011;278:1489-1497.
- Fujikado T, Kamei M, Sakaguchi H, et al. Testing of semi-chronically implanted retinal prosthesis by suprachoroidal-transretinal stimulation in patients with retinitis pigmentosa. *Invest Ophthalmol Vis Sci*. 2011;52:4726-4733.
- Morimoto T, Miyoshi T, Fujikado T, Tano Y, Fukuda Y. Electrical stimulation enhances the survival of axotomized retinal ganglion cells in vivo. *NeuroReport*. 2002;13:227-230.
- Morimoto T, Miyoshi T, Matsuda S, Tano Y, Fujikado T, Fukuda Y. Transcorneal electrical stimulation rescues axotomized retinal ganglion cells by activating endogenous retinal IGF-1 system. *Invest Ophthalmol Vis Sci*. 2005;46:2147-2155.
- Morimoto T, Miyoshi T, Sawai H, Fujikado T. Optimal parameters of transcorneal electrical stimulation (TES) to be neuroprotective of axotomized RGCs in adult rats. *Exp Eye Res*. 2010;90:285-291.
- Miyake K, Yoshida M, Inoue Y, Hata Y. Neuroprotective effect of transcorneal electrical stimulation on the acute phase of optic nerve injury. *Invest Ophthalmol Vis Sci*. 2007;48:2356-2361.
- Tagami Y, Kurimoto T, Miyoshi T, Morimoto T, Sawai H, Mimura O. Axonal regeneration induced by repetitive electrical stimulation of crushed optic nerve in adult rats. *Jpn J Ophthalmol*. 2009;53:257-266.
- Fujikado T, Morimoto T, Matsushita K, Shimojo H, Okawa Y, Tano Y. Effect of transcorneal electrical stimulation in patients with nonarteritic ischemic optic neuropathy or traumatic optic neuropathy. *Jpn J Ophthalmol*. 2006;50:266-273.
- Morimoto T, Fujikado T, Choi JS, et al. Transcorneal electrical stimulation promotes the survival of photoreceptors and preserves retinal function in royal college of surgeons rats. *Invest Ophthalmol Vis Sci*. 2007;48:4725-4732.
- Ni YQ, Gan DK, Xu HD, Xu GZ, Da CD. Neuroprotective effect of transcorneal electrical stimulation on light-induced photoreceptor degeneration. *Exp Neurol*. 2009;219:439-452.
- Schatz A, Röck T, Naycheva L, et al. Transcorneal electrical stimulation for patients with retinitis pigmentosa: a prospective, randomized, sham-controlled exploratory study. *Invest Ophthalmol Vis Sci*. 2011;52:4485-4496.
- Daiger SP, Bowne SJ, Sullivan LS. Perspective on genes and mutations causing retinitis pigmentosa. *Arch Ophthalmol*. 2007;125:151-158.
- Kondo M, Sakai T, Komeima K, et al. Generation of a transgenic rabbit model of retinal degeneration. *Invest Ophthalmol Vis Sci*. 2009;50:1371-1377.
- Oh KT, Longmuir R, Oh DM, et al. Comparison of the clinical expression of retinitis pigmentosa associated with rhodopsin mutations at codon 347 and codon 23. *Am J Ophthalmol*. 2003;136:306-313.
- Berson EL, Rosner B, Sandberg MA, et al. Ocular findings in patients with autosomal dominant retinitis pigmentosa and rhodopsin, proline-347-leucine. *Am J Ophthalmol*. 1991;111:614-623.
- Sakai T, Kondo M, Ueno S, et al. Supernormal ERG oscillatory potentials in transgenic rabbit with rhodopsin P347L mutation

- and retinal degeneration. *Invest Ophthalmol Vis Sci.* 2009;50:4402-4409.
24. Bush RA, Lei B, Tao W, et al. Encapsulated cell-based intraocular delivery of ciliary neurotrophic factor in normal rabbit: dose-dependent effects on ERG and retinal histology. *Invest Ophthalmol Vis Sci.* 2004;45:2420-2430.
 25. D'Cruz PM, Yasumura D, Weir J, et al. Mutation of the receptor tyrosine kinase gene *Mertk* in the retinal dystrophic RCS rat. *Hum Mol Genet.* 2000;9:645-651.
 26. Noell WK, Walker VS, Kang BS, Berman S. Retinal damage by light in rats. *Invest Ophthalmol.* 1966;5:450-473.
 27. Jones BW, Kondo M, Terasaki H, et al. Retinal remodeling in the Tg P347L rabbit, a large-eye model of retinal degeneration. *J Comp Neurol.* 2011;519:2713-2733.
 28. Léveillard T, Mohand-Saïd S, Lorentz O, et al. Identification and characterization of rod-derived cone viability factor. *Nat Genet.* 2004;36:755-759.
 29. Willmann G, Schäferhoff K, Fischer MD, et al. Gene expression profiling of the retina after transcorneal electrical stimulation in wildtype brown Norway rats. *Invest Ophthalmol Vis Sci.* 2011;52:7529-7537.
 30. Sato T, Lee TS, Takamatsu F, Fujikado T. Induction of fibroblast growth factor-2 by electrical stimulation in cultured retinal Müller cells. *Neuroreport.* 2008;19:1617-1621.
 31. Sato T, Fujikado T, Morimoto T, Matsushita K, Harada T, Tano Y. Effect of electrical stimulation on IGF-1 transcription by L-type calcium channels in cultured retinal Müller cells. *Jpn J Ophthalmol.* 2008;52:217-223.
 32. Sato T, Fujikado T, Lee TS, Tano Y. Direct effect of electrical stimulation on induction of brain-derived neurotrophic factor from cultured retinal Müller cells. *Invest Ophthalmol Vis Sci.* 2008;49:4641-4646.
 33. Ciavatta VT, Kim M, Wong P, et al. Retinal expression of Fgf2 in RCS rats with subretinal microphotodiode array. *Invest Ophthalmol Vis Sci.* 2009;50:4523-4530.
 34. Kurimoto T, Oono S, Oku H, et al. Transcorneal electrical stimulation increases chorioretinal blood flow in normal human subjects. *Clin Ophthalmol.* 2010;4:1441-1446.
 35. Mihashi T, Okawa Y, Miyoshi T, Kitaguchi Y, Hirohara Y, Fujikado T. Comparing retinal reflectance changes elicited by transcorneal electrical retinal stimulation with those of optic chiasma stimulation in cats. *Jpn J Ophthalmol.* 2011;55:49-56.
 36. Inomata K, Shinoda K, Ohde H, et al. Transcorneal electrical stimulation of retina to treat longstanding retinal artery occlusion. *Graefes Arch Clin Exp Ophthalmol.* 2007;45:1773-1780.
 37. Oono S, Kurimoto T, Kashimoto R, Tagami Y, Okamoto N, Mimura O. Transcorneal electrical stimulation improves visual function in eyes with branch retinal artery occlusion. *Clin Ophthalmol.* 2011;5:397-402.
 38. Spalton DJ, Bird AC, Cleary PE. Retinitis pigmentosa and retinal oedema. *Br J Ophthalmol.* 1978;62:174-182.
 39. Uliss AE, Gregor ZJ, Bird AC. Retinitis pigmentosa and retinal neovascularization. *Ophthalmology.* 1986;93:1599-1602.
 40. Matthes MT, Bok D. Blood vascular abnormalities in the degenerative mouse retina (C57BL/6J-rd1e). *Invest Ophthalmol Vis Sci.* 1984;25:364-369.
 41. Wang S, Villegas-Pérez MP, Vidal-Sanz M, Lund RD. Progressive optic axon dystrophy and vascular changes in rd mice. *Invest Ophthalmol Vis Sci.* 2000;41:537-545.

Real-Time Imaging of Rabbit Retina with Retinal Degeneration by Using Spectral-Domain Optical Coherence Tomography

Yuki Muraoka¹, Hanako Ohashi Ikeda^{1*}, Noriko Nakano¹, Masanori Hangai¹, Yoshinobu Toda², Keiko Okamoto-Furuta², Haruyasu Kohda², Mineo Kondo³, Hiroko Terasaki⁴, Akira Kakizuka⁵, Nagahisa Yoshimura¹

1 Department of Ophthalmology and Visual Sciences, Kyoto University Graduate School of Medicine, Kyoto, Japan, **2** Center for Anatomical Studies, Kyoto University Graduate School of Medicine, Kyoto, Japan, **3** Department of Ophthalmology, Mie University School of Medicine, Tsu, Japan, **4** Department of Ophthalmology, Nagoya University Graduate School of Medicine, Nagoya, Japan, **5** Laboratory of Functional Biology, Kyoto University Graduate School of Biostudies and Solution Oriented Research for Science and Technology, Kyoto, Japan

Abstract

Background: Recently, a transgenic rabbit with rhodopsin Pro 347 Leu mutation was generated as a model of retinitis pigmentosa (RP), which is characterized by a gradual loss of vision due to photoreceptor degeneration. The purpose of the current study is to noninvasively visualize and assess time-dependent changes in the retinal structures of a rabbit model of retinal degeneration by using speckle noise-reduced spectral-domain optical coherence tomography (SD-OCT).

Methodology/Principal Findings: Wild type (WT) and RP rabbits (aged 4–20 weeks) were investigated using SD-OCT. The total retinal thickness in RP rabbits decreased with age. The thickness of the outer nuclear layer (ONL) and between the external limiting membrane and Bruch's membrane (ELM–BM) were reduced in RP rabbits around the visual streak, compared to WT rabbits even at 4 weeks of age, and the differences increased with age. However, inner nuclear layer (INL) thickness in RP rabbits did not differ from that of WT during the observation period. The ganglion cell complex (GCC) thickness in RP rabbits increased near the optic nerve head but not around the visual streak in the later stages of the observation period. Hyper-reflective change was widely observed in the inner segments (IS) and outer segments (OS) of the photoreceptors in the OCT images of RP rabbits. Ultrastructural findings in RP retinas included the appearance of small rhodopsin-containing vesicles scattered in the extracellular space around the photoreceptors.

Conclusions/Significance: In the current study, SD-OCT provided the pattern of photoreceptor degeneration in RP rabbits and the longitudinal changes in each retinal layer through the evaluation of identical areas over time. The time-dependent changes in the retinal structure of RP rabbits showed regional and time-stage variations. *In vivo* imaging of RP rabbit retinas by using SD-OCT is a powerful method for characterizing disease dynamics and for assessing the therapeutic effects of experimental interventions.

Citation: Muraoka Y, Ikeda HO, Nakano N, Hangai M, Toda Y, et al. (2012) Real-Time Imaging of Rabbit Retina with Retinal Degeneration by Using Spectral-Domain Optical Coherence Tomography. PLoS ONE 7(4): e36135. doi:10.1371/journal.pone.0036135

Editor: Steven Barnes, Dalhousie University, Canada

Received: November 27, 2011; **Accepted:** March 26, 2012; **Published:** April 27, 2012

Copyright: © 2012 Muraoka et al. This is an open-access article distributed under the terms of the Creative Commons Attribution License, which permits unrestricted use, distribution, and reproduction in any medium, provided the original author and source are credited.

Funding: This research was supported by Research grants from the Astellas Foundation for Research on Metabolic Disorders and the Japan Foundation for Applied Enzymology, and a Grant-in-Aid for Young Scientists (22791656) from the Ministry of Education, Culture, Sports, Science and Technology (MEXT). The funders had no role in study design, data collection and analysis, decision to publish, or preparation of the manuscript.

Competing Interests: The authors have declared that no competing interests exist.

* E-mail: hanakoi@kuhp.kyoto-u.ac.jp

Introduction

Retinitis pigmentosa (RP) is an inherited retinal disorder characterized by a progressive loss of visual function due to degeneration of rod and cone photoreceptors and eventual atrophy of the entire retina [1,2]. However, there are no effective treatments for RP. Various animal models of RP have been developed and studied to elucidate the pathophysiology of the disease and to develop new treatments [3–10]. Of these models, only monkeys have a macula, an important area for vision due to the high density of cone photoreceptors. However, it is not easy to study the pathophysiology of RP in monkeys due to handling and

breeding difficulties. Rabbits are known to have a visual streak, where the rod and cone photoreceptor density is highest, about 3 mm ventral to the optic nerve head (ONH) [11,12]. Rabbits are easy to breed and handle, and the physiology and morphology of rabbit retina is well understood [11–14]. Additionally, in mid-sized animals like rabbits, surgical treatments such as subretinal injection of cells for regenerative therapy [15,16], vectors for gene therapy [17], and implantation of intraocular devices [18,19] are easily performed. Therefore, rabbits are very useful for studying retinal diseases and testing new therapeutic interventions. For these reasons, we used transgenic (Tg) rabbits with mutated rhodopsin (Pro 347 Leu, RP rabbits) as a mid-sized model for RP

[20] to study the pathophysiology and develop new evaluation systems for retinal degeneration.

Optical coherence tomography (OCT) devices allow non-invasive detection of retinal architecture, including quantitative measurements of retinal thickness and longitudinal observation of the retinal architecture [21]. The technological advances in spectral-domain OCT (SD-OCT) have enabled high-speed scanning and improved image resolution [22]. Furthermore, the exact averaging of B-scans with a three-dimensional eye-tracking system and high-speed scanning have enabled sufficient reduction in speckle noise, the most influential artificial noise that blurs the boundaries between retinal layers [23,24]. These advances have improved visualization of individual retinal layers, including both the outer retina and the inner retina (i.e., ganglion cell layer and inner plexiform layer [IPL] in humans) [25,26]. SD-OCT imaging also enables evaluation of the junction between the inner segment (IS) and the outer segment (OS) of the photoreceptors (IS/OS) [27–29] and that of the external limiting membrane (ELM) [30,31] as hallmarks of photoreceptor integrity. That is, visual function can be speculated from OCT images to some extent. Thus, the use of OCT imaging in humans has contributed to a more detailed understanding of the pathophysiology of many retinal diseases. In mice, the retina has been clearly visualized using SD-OCT [32–37]. Thus, in experimental animals, SD-OCT may allow *in vivo* detection and monitoring of changes in retinal architecture without sacrificing animals.

In mouse models of retinal degeneration, Fischer [36] and Huber et al. [32] detected and analyzed photoreceptor degeneration by using SD-OCT. They imaged the thinning of inner

retinal layers and compared the total retinal thickness with that of normal mice in several mouse RP models. Yamauchi et al. reported the retinal architecture of rabbits by using SD-OCT following iodoacetic acid-induced photoreceptor degeneration [38]. However, retinal pathomorphology of genetically engineered rabbit models of RP, which mimic human RP [20], and longitudinal assessment of changes in the individual retinas remain to be studied with SD-OCT.

The purpose of this study was to visualize the time-dependent changes in photoreceptors, elucidate the pattern of changes in each retinal layer around the visual streak in identical eyes of RP rabbits by using SD-OCT, and assess the visual functions by electroretinography (ERG).

Results

Visualization of retinal structures in RP rabbits with SD-OCT

We first investigated whether the retinal structures of WT rabbits could be clearly visualized using SD-OCT. Vertical OCT images, which passed through the center of the ONH (Fig. 1A), permitted clear identification of each retinal layer, the choroid, and sclera of WT rabbits (Figs. 1B and 1C). The ELM and IS/OS lines were also clearly identifiable, the integrity of which have been shown to be positively associated with visual function. In the vertical OCT images, the scleral ring was defined as the edge of the ONH so that OCT measurements could be longitudinally compared between each rabbit and between WT and RP rabbits (Fig. 1B).

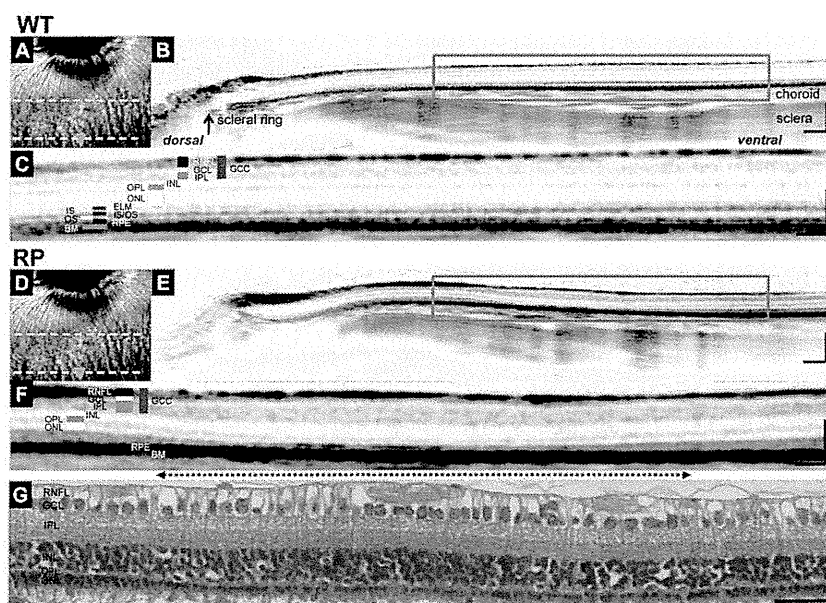


Figure 1. SD-OCT images of WT and Retinitis Pigmentosa (RP) rabbit retinas and histology of the visual streak in an RP rabbit. (A) A fundus infrared image of a WT rabbit retina, including optic nerve head (ONH) and visual streak. The area between dotted lines is the visual streak. (B) A vertical SD-OCT image along the green arrow in panel A, which passes through the center of the ONH. On this vertical image, the scleral ring was regarded as the lower margin of the ONH. (C) A magnified OCT image of the area enclosed by the blue square in panel B, which includes the visual streak. (D) A fundus infrared image of a RP rabbit retina, including the ONH and visual streak. (E) A vertical SD-OCT image of a 20-week-old RP rabbit along the green arrow in panel D. (F) A magnified OCT image of the area enclosed by the blue square in panel E. The 2.2 mm width of this OCT section was vertically cut between 1.8 mm and 4.0 mm ventral to the inferior edge of the ONH. A dotted arrow indicates the region of the visual streak. (G) Hematoxylin-Eosin staining of a retinal section corresponding to the area in the OCT image in F. Scale Bar = 200 μ m (B, E), 100 μ m (C, F), and 50 μ m (G). RNFL, retinal nerve fiber layer; GCL, ganglion cell layer; IPL, inner plexiform layer; GCC, ganglion cell complex; INL, inner nuclear layer; OPL, outer plexiform layer; ONL, outer nuclear layer; ELM, external limiting membrane; IS, inner segments of photoreceptors; OS, outer segments of photoreceptors; IS/OS, junctions between IS and OS; RPE, retinal pigment epithelium; and BM, Bruch's membrane.
doi:10.1371/journal.pone.0036135.g001

Next, we examined a 20-week-old RP rabbit that expressed mutated rhodopsin (Figs. 1D–1F). The outer nuclear layer (ONL) of the RP rabbit was much thinner than the WT rabbit. Furthermore, in the RP rabbit, the photoreceptors around the visual streak (indicated by the dotted arrow), where the densities of rod and cone photoreceptors were the highest, appeared to be more severely damaged than in any other area. In this area, the ONL was very thin and the outer plexiform layer (OPL) was faint or absent depending on the distance from the ONH and the IS/OS line was undetectable (Fig. 1F). This regional variation in photoreceptor damage was also detected with hematoxylin and eosin (H&E) staining in the same eye (Fig. 1G).

Time-dependent changes in the photoreceptor layers and in the visual function of RP rabbits

As observations revealed that photoreceptor damage was severe around the visual streak, we were encouraged to investigate the time-dependent changes in the photoreceptors of identical RP rabbits beneath the visual streak with SD-OCT and compared them with those of the WT rabbits (Fig. 2A). At 4 weeks of age (with the youngest that can be examined by OCT), the ONL of RP rabbits was almost as thick as WT rabbits. Following 4 weeks of age, the ONL thickness in RP rabbits decreased. At 20 weeks, the ONL thickness in RP rabbits was much smaller than in WT

rabbits. Photoreceptor IS and OS, where visual phototransduction occurs, were thin in RP rabbits. In contrast, the architecture of the inner retina was relatively preserved in RP rabbits at both 10 and 20 weeks of age.

In the current SD-OCT study, there were additional findings in the photoreceptor layers. In the sections of WT rabbits, the reflectivity of IS and OS was low compared to that of the ELM and IS/OS lines. In contrast, the IS and OS were highly reflective in RP rabbits, and almost equivalent to the ELM and IS/OS lines throughout the study ages (Fig. 2A).

To compare the SD-OCT data with those from the histological examination, histological sections of the age-matched RP and WT rabbits were prepared (Fig. 2B). The number of photoreceptors and thickness of the ONL, IS, and OS in the RP rabbits decreased with age, which is consistent with those of a previous report [20]. At 20 weeks of age, the nuclei of photoreceptors in RP rabbits were reduced to 1 or 2 rows, which was much less compared to WT rabbits. The magnitude of the decrease in ONL thickness appears similar between the histological and SD-OCT data (Figs. 2A and 2B). In the histological sections of a 4-week-old RP rabbit, the total retinal thickness and the ONL thickness were almost the same as those of the WT rabbit, and the IS and OS appeared intact. The high reflectivity in the IS and OS observed in the OCT sections was difficult to explain by the histological sections (Figs. 2A and 2B).

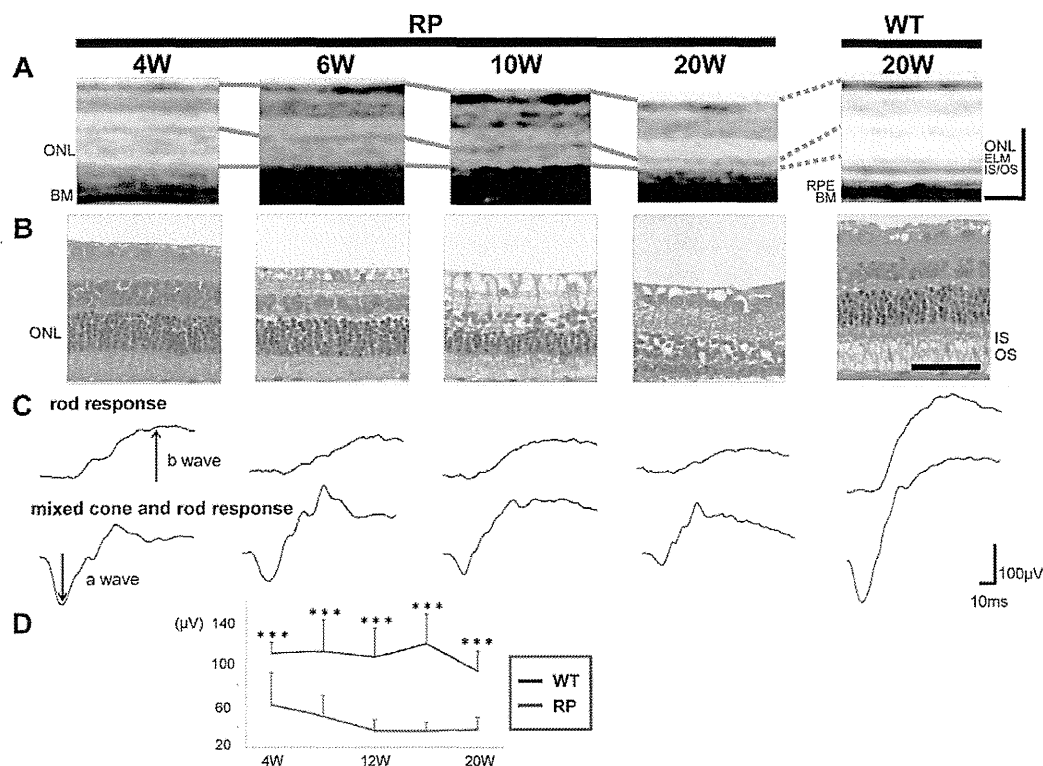


Figure 2. Time-dependent changes in morphological features of the retina and visual function in the RP rabbits. (A) SD-OCT images beneath the visual streak in an RP rabbit at 4, 6, 10, and 20 weeks and in a 20-week-old WT rabbit. The total retinal and ONL thickness in the RP rabbits decreased with age. The IS and OS were highly reflective in the RP rabbits compared with the WT rabbits. ONL, outer nuclear layer; and OS, outer segments of photoreceptors. (B) Hematoxylin-eosin staining of retinas in 4-, 6-, 10-, and 20-week-old RP and 20-week-old WT rabbits. The ONL in RP rabbits thinned with age. In 20-week-old RP rabbits, only 1–2 layers of nuclei were detected in the ONL. (C) Representative scotopic electroretinograms of 4-, 6-, 10-, and 20-week-old RP and 20-week-old WT rabbits. (D) The a-wave amplitude of the mixed rod and cone response. The amplitude was smaller in the RP rabbits than in the WT rabbits. The differences between the WT and RP rabbits were significant at all study points between 4 and 20 weeks. * $P < 0.05$, *** $P < 0.001$ (unpaired *t*-test). Scale Bar = 100 μm in A, and 50 μm in B. ONL, outer nuclear layer; ELM, external limiting membrane; IS/OS, junctions between inner segment (IS) and outer segment (OS); RPE, retinal pigment epithelium; and BM, Bruch's membrane.

doi:10.1371/journal.pone.0036135.g002

Next, to evaluate visual function of the rod and cone systems of RP rabbits, scotopic full-field ERG was recorded (Fig. 2C). The a-wave of the mixed cone and rod response, which mainly originates from the photoreceptors, was smaller in RP rabbits ($61.2 \pm 30.5 \mu\text{V}$) (mean \pm SD) than in WT rabbits ($110.3 \pm 10.7 \mu\text{V}$; $P = 0.010$, unpaired *t*-test) as early as 4 weeks. The a-wave amplitude was reduced with RP rabbit aged (Fig. 2D). At the age of 20 weeks, the a-wave amplitude decreased to $37.6 \pm 11.5 \mu\text{V}$ in RP rabbits and was significantly less than that of WT rabbits ($93.5 \pm 19.0 \mu\text{V}$; $P < 0.001$, unpaired *t*-test, Figs. 2C and 2D). The b-wave amplitude of the rod response, which originates indirectly from bipolar and Müller cells, was $97.3 \pm 33.2 \mu\text{V}$ in RP rabbits and was less than that of WT rabbits ($280.8 \pm 71.3 \mu\text{V}$; $P < 0.001$, unpaired *t*-test, Fig. 2C). These data suggest that the visual function of both the rod and cone systems was disturbed in RP rabbits, consistent with a previous report [20]. These results indicate that loss of photoreceptors and concomitant visual dysfunction gradually occurs in RP rabbits.

Vesicles cleaved from photoreceptors and disorganization of IS and OS in RP rabbits account for the hyper-reflectivity seen in SD-OCT images

To elucidate the cause of the hyper-reflective change in the outer photoreceptor layers of RP rabbits in SD-OCT sections, we examined and compared the ultrastructure of the retina between RP and WT rabbits at 4 or 20 weeks of age. In WT rabbits, the IS and OS exhibited a dense and regular arrangement (Figs. 3A, 3B, S1A and S1B). In contrast, in the RP retinas, the IS and OS were less organized at 4 weeks of age (Figs. 3C and 3D), and they were mostly absent at 20 weeks of age (Figs. S1C and S1D). Magnified images of the RP retinas revealed large number of small,

approximately 100 nm, vesicles scattered in the extracellular space around the photoreceptors (arrowheads in Fig. 3D and S1D). These small vesicles appeared to be cleaved from the membrane of the IS in RP rabbits (arrows in Fig. 3E and S1D). The disrupted organization and the presence of vesicles between the IS and OS on ultra microscopy may account for the hyper-reflectivity seen in the corresponding area of the SD-OCT images.

To determine the origin of the vesicles, we performed ultrastructural immunohistochemistry by using monoclonal antibodies against rhodopsin (Fig. 3F). In RP retinas, numerous vesicles with dots were observed, indicating the presence of rhodopsin within the vesicles (disintermediated arrowheads in Fig. 3F).

Time-dependent changes in the individual retinal layers in SD-OCT sections exhibit regional and time-stage variations in RP rabbits

In the SD-OCT examinations, the retinal thickness in the RP rabbits appeared to decrease with age. Therefore, we quantitatively measured the mean total retinal thickness around the visual streak in the WT and RP rabbits (Figs. 4A and S2). As shown in Fig. 4A, the total retinal thickness in WT rabbits did not change with age, whereas that of the RP rabbits progressively decreased. The total retinal thickness in WT and RP rabbits was not significantly different at 4 weeks. However, after 6 weeks, the differences in the total retinal thickness increased and continued with age. At 20 weeks, the total retinal thickness in RP rabbits was $165.8 \pm 8.5 \mu\text{m}$ and significantly smaller than that of WT rabbits ($194.3 \pm 7.7 \mu\text{m}$; $P < 0.001$, unpaired *t*-test).

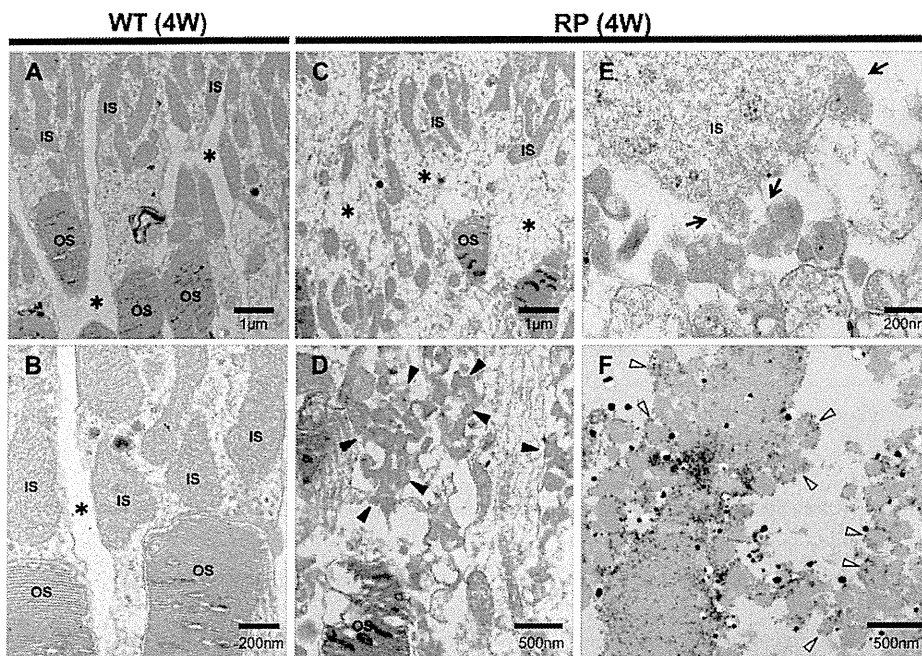


Figure 3. Ultrastructure of photoreceptors in WT and RP rabbits. (A, B) Ultrastructure of photoreceptors in 4-week-old WT rabbits. The inner (IS) and outer segments (OS) of the photoreceptors were regular and dense. There are no vesicles in the extracellular spaces (*). (C–E) Ultrastructure of the photoreceptors in the 4-week-old RP rabbits. The IS and OS were less organized than those in the WT rabbits. In the magnified image (D), the RP rabbit retina showing many small vesicles (arrowheads) accumulated in the extracellular spaces (indicated with * in panel C). The vesicles appeared to be cleaved from the IS into the extracellular space around the photoreceptors (arrows in panel E). (F) Ultrastructural immunohistochemistry by using an anti-rhodopsin antibody. The small vesicles (disintermediated arrowheads) in the extracellular spaces around the photoreceptors exhibit black dots indicating the presence of rhodopsin.

doi:10.1371/journal.pone.0036135.g003

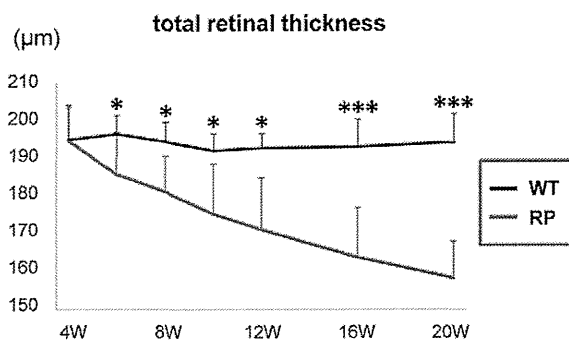


Figure 4. Time-dependent changes in total retinal thickness, and mixed cone and rod response in the WT and RP rabbits. The total retinal thickness was measured within a circle 1 mm in diameter 3 mm ventral to the lower margin of the ONH and averaged. The total retinal thickness in the WT rabbits (indicated with a blue line) was unchanged during observation, whereas that in the RP rabbits (indicated with a red line) severely decreased with age. * $P < 0.05$, *** $P < 0.001$ (unpaired *t*-test). doi:10.1371/journal.pone.0036135.g004

OCT examination showed that the photoreceptors were most severely damaged at the visual streak, approximately 3 mm ventral to the ONH [11]. Therefore, we longitudinally examined regional and periodical variations in the progression of retinal degeneration in RP rabbits. For this purpose, we measured the thickness of each retinal layer within 0.5-mm areas 4 mm ventral to the lower edge of the ONH as a function of distance from the lower optic disc margin at 4, 6, 10, and 20 weeks by using the vertical OCT images that passed through the center of the ONH and visual streaks (Fig. 5B).

ONL thickness. We first evaluated the thickness of the ONL where the nuclei of photoreceptors are located (Fig. 5A). In WT rabbits, the ONL in each area became slightly thinner with age. In younger WT rabbits (4–6 weeks old), the ONL was thinner in areas more distant from the ONH. In RP rabbits, the decrease in ONL thickness with age was more progressive than that of WT rabbits. At any age examined, thinning of the ONL was greater in areas more distant from the ONH. At 10 and 20 weeks, the ONL was thinnest in the area 3.0–3.5 mm ventral to the ONH.

At 4 weeks, the ONL thickness in RP rabbits was significantly less than that of WT rabbits in only the area 3.0–3.5 mm from the ONH ($P = 0.037$, unpaired *t*-test). Areas that exhibited a difference in ONL thickness between WT and RP rabbits expanded with age. At 20 weeks, the ONL thickness in RP rabbits was significantly smaller than that of WT rabbits in each of the 7 areas examined ($P < 0.001$, unpaired *t*-test, Fig. 5E).

ELM–BM thickness. The ELM–BM thickness was evaluated because the area between the ELM and BM includes the length of the IS and OS where visual phototransduction occurs (Figs. 5B and S3). In WT rabbits, the ELM–BM thickness was larger in areas more distant from the ONH at any age examined. On the other hand, in RP rabbits, the differences in the ELM–BM thickness between areas as a function of distance from the ONH were smaller compared to those of WT rabbits at 4–10 weeks; the ELM–BM thickness appeared to decrease mainly in the areas distant from the optic disc. In 20-week-old RP rabbits, the ELM–BM thickness markedly decreased in the area 2.5–3.5 mm ventral to the ONH and was significantly less than that in the corresponding areas in WT rabbits ($P < 0.001$, unpaired *t*-test, Fig. 5E).

INL thickness. The INL comprises the nuclei of bipolar, horizontal, amacrine, and Müller cells. The INL thickness was larger in areas more distant from the ONH in both WT and RP

rabbits at the ages of 4 to 20 weeks (Fig. 5C). The INL thickness in WT and RP rabbits was not significantly different in each corresponding area at all the ages examined (Fig. 5E).

GCC thickness. The GCC consists of the retinal nerve fiber layer (axons of ganglion cells), ganglion cell layer (somata of ganglion cells), and IPL. To determine the influence of photoreceptor degeneration on the inner retina, GCC thickness was measured (Figs. S3 and 5D). The GCC thickness in the WT and RP rabbits exhibited a similar pattern in all the areas examined at the ages of 4 and 6 weeks. However, in 20-week-old RP rabbits, the GCC thickness in the areas close to the ONH was larger than in younger RP rabbits and in the corresponding areas of 20-week-old WT rabbits ($P < 0.001$ for both, unpaired *t*-test, Fig. 5E).

In summary, the decrease in the ONL and ELM–BM thickness in RP rabbits was first detected in the areas approximately 3.0 mm ventral to the lower edge of the ONH (areas corresponding to the visual streak). Thinning of the IS and OS (measured as the ELM–BM thickness) followed thinning of the ONL. In contrast, the INL thickness in RP rabbits did not change throughout the observational period of 4 to 20 weeks. The GCC thickness in RP rabbits increased in areas away from the visual streaks but close to the ONH in the later phase of observation (Fig. 5E).

Discussion

In this study, we examined time-dependent changes in photoreceptor degeneration in identical RP rabbits, and compared the pattern of changes in individual retinal layers between WT and RP rabbits for the first time by using SD-OCT. In RP rabbits, we observed regional differences in the degree of photoreceptor loss. That is, the ONL (ONL: the somata of photoreceptors) in RP rabbits was thinnest beneath the visual streak, where the densities of rod and cone photoreceptors were the highest in WT rabbits, and the photoreceptors of RP rabbits were relatively preserved in the area near the ONH. The current observations by using SD-OCT revealed longitudinal changes in the RP rabbit retina that were fairly consistent with a previous histological study of the RP rabbits [20] and reports based on other animal models of RP [3,9].

To elucidate the unique “highly reflective IS and OS” feature of the outer photoreceptor layer during photoreceptor degeneration in RP rabbits, an electron microscopy study was conducted on 4- or 20-week-old RP rabbits. We detected vesicles around the photoreceptors and loss of most of the IS and OS. We speculate that these destructive structures in RP rabbits cause the hyper-reflectivity seen in the outer photoreceptor layers (between ELM and BM) on SD-OCT images (Fig. 2A). The vesicles appeared to be cleaved from the IS, as described in a previous report [20]. Moreover, these vesicles were shown to include rhodopsin by ultrastructural immunohistochemistry (Fig. 3F), indicating that the particles were derived from photoreceptors. In SD-OCT images of 4-week-old RP rabbits, the area between the ELM and BM was hyper-reflective even though the reflectivity and the thickness of the ONL were unchanged (Fig. 2A). These observations point to the mechanism by which photoreceptors degenerate in RP rabbits. That is, defective transport of rhodopsin from the IS to the OS, which was demonstrated in mice with mutated rhodopsin P347S by using an antibody against the mutated rhodopsin [39], is followed by cleavage of vesicles from the IS, and finally cell bodies of photoreceptors degenerate. It is speculated that early stage RP patients may have mutations in the rhodopsin gene if hyper-reflective patterns are detected with SD-OCT in the area corresponding to the IS and OS, though further studies are needed to confirm this speculation.

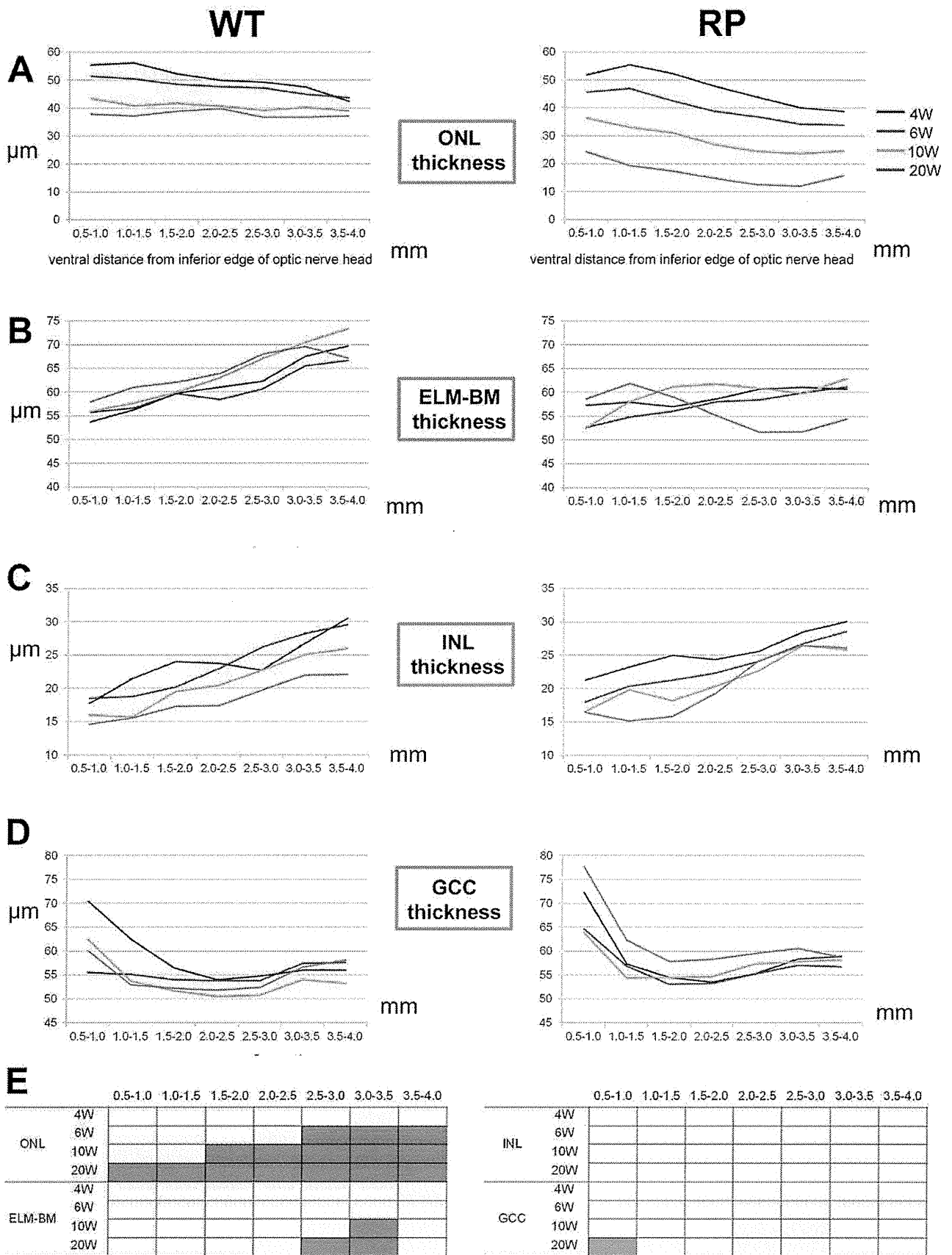


Figure 5. Time-dependent changes in the thickness of individual retinal layers in WT and RP rabbits. (A–D) Time-dependent changes in ONL (A), ELM–BM (B), INL (C), and GCC (D) thickness measured with vertical OCT sections of WT and RP rabbits. Mean values at 4, 6, 10, and 20 weeks are indicated with blue, red, green, and purple lines, respectively. X-axes indicate the distance from the inferior edge of the ONH. (E) A schema to show time course and regional variations in the thickness of each retinal layer in RP rabbits from 4 to 20 weeks. Blue color indicates the regions where retinal thickness of RP rabbits was significantly smaller than that of WT rabbits. Orange color indicates the regions where retinal thickness of RP rabbits was significantly larger than that of WT rabbits. Deep and light colors indicate $P < 0.001$ and $P < 0.05$, respectively (unpaired *t*-test). ONL, outer nuclear layer; ELM, external limiting membrane; BM, Bruch’s membrane; INL, inner nuclear layer; and GCC, ganglion cell complex.
doi:10.1371/journal.pone.0036135.g005

Aleman et al. reported the following disease sequence in human and murine RP caused by mutation of the rhodopsin gene: ONL diminution with INL thickening, amalgamation of residual ONL with the thickened INL, and progressive retinal remodeling with eventual thinning seen in OCT [40]. In our SD-OCT study, the INL thickness was not significantly different between WT and RP rabbits at the ages of 4 to 20 weeks. In contrast, the GCC thickness in RP rabbits paradoxically increased in the later phase of observation. Previous studies have suggested that the increase in the INL/inner retinal thickness in patients with RP maybe related to Müller glial activation with hypertrophy [40–42]. In the current study with RP rabbits, the observational period may be too short to detect an increase in INL thickness, or the gliosis of Müller cells may occur preferably within the GCC than in the INL.

This study has some limitations. The area imaged with SD-OCT was quite restricted such that the degeneration in RP retinas obtained with SD-OCT did not always correlate with the total retinal function. Furthermore, OCT or ERG could not be performed on rabbits younger than 4 weeks as their eyelids had not yet opened.

In conclusion, despite these short comings, *in vivo* time-dependent changes in the retinal structures were seen layer-by-layer in RP rabbits by using SD-OCT. These changes in the retinal structure had regional and temporal variations not only in the outer retina but also in the inner retina of RP rabbits. This study demonstrates that *in vivo* imaging with SD-OCT can facilitate the characterization of morphological disease dynamics and serve as a powerful tool for developing new treatments, such as gene therapy, intraocular devices, and neuroprotective treatments, in rabbit models of RP.

Methods

Experimental animals

This study was conducted in accordance with the Association Research in Vision and Ophthalmology (ARVO) Statement for the Use of Animals in Ophthalmic and Vision Research. All the protocols were approved by the Institutional Review Board of the Kyoto University Graduate School of Medicine (MedKyo11229).

New Zealand White rabbits (NZW, WT) and RP rabbits with rhodopsin P347L mutation (NZW, RP) [20] were purchased from Kitayama Labes Co., Ltd (Ina, Nagano, Japan). All rabbits were kept under a 14 h–10 h light-dark cycle (approximately 200 lux), given free access to water, and fed once a day. For the ERG recording and SD-OCT image acquisition, male WT ($n = 4$ –10 eyes) and RP rabbits ($n = 10$ –16 eyes) were used.

Retinal histology

Rabbit eyes were fixed overnight in a mixture of 10% neutral buffered formalin and 2.5% glutaraldehyde and then transferred to 10% neutral buffered formalin. The tissues were trimmed, embedded in paraffin, sectioned vertically through the optic nerve (superior-inferior), and stained with hematoxylin and eosin. The retina beneath the visual streak was examined and compared between 10- and 20-week-old WT and RP rabbits.

ERG

ERG was performed to assess the visual function of WT and RP rabbits at 4, 6, 10, and 20 weeks. Pupils were dilated with tropicamide (0.5%) and phenylephrine (0.5%) eye drops. Rabbits were dark-adapted for more than 60 min before anesthetization with an intramuscular injection of ketamine (25 mg/kg) and xylazine (2 mg/kg). ERG was recorded using a gold loop corneal electrode with a light-emitting diode (Mayo Corp., Inazawa, Japan). A reference electrode was placed in the mouth, and a ground electrode was attached to the ear. Stimuli were produced with a light-emitting diode stimulator (Mayo Corp.). The ERG response signals were amplified, digitized at 10 kHz with a band-pass filter of 0.3 to 500 Hz and analyzed (PowerLab 2/25; AD instruments, New South Wales, Australia). Two steps of stimulus intensities (ISCEV standard; scotopic 0.01 and scotopic 3.0) were used for evaluating rod and mixed cone and rod responses. The b-wave amplitude of the rod response and the a-wave amplitude of the mixed cone and rod response were analyzed.

SD-OCT

After ERG recording, rabbits were placed on a platform such that the visual streaks, which were approximately 3 mm ventral to the ONH, were located at the center of the image. The SD-OCT machine used in this study was *Multiline* OCT (Heidelberg Engineering, Heidelberg, Germany), which was customized based on a Spectralis HRA+OCT [37]. The *Multiline* OCT uses an 870-nm super-luminescent diode as a light source. The scan rate of the SD-OCT was 47,000 A-scans per second, with an axial resolution of $\sim 7 \mu\text{m}$.

Measurement and evaluations of total retinal thickness by using SD-OCT

To measure the total retinal thickness at the visual streak, a volume scan image was obtained (Fig. S2A). The lines of the vitreoretinal interface and BM were manually delineated at each horizontal section in a masked fashion (Figs. S2B and S2C). The mean total retinal thickness was measured within a red circle 1 mm in diameter, the center of which was 3 mm ventral to the inferior edge of the ONH, as determined by the software supplied by Heidelberg Engineering (Figs. S2D and S2E).

Measurements and evaluation of the thickness of retinal layers on vertical SD-OCT images

To measure and assess the thickness of each retinal layer, vertical OCT images, which passed through the center of the ONH and included the visual streak, were obtained by averaging 100 B-scans. To measure the thickness of the ONL, ELM–BM, INL, and GCC, the boundary lines between the OPL and ONL, ELM and BM, IPL and INL, and the vitreoretinal interface and IPL were manually delineated in a masked fashion (Fig. S3). The thickness of each retinal layer within the areas (0.5 mm each) 4 mm ventral to the lower edge of the ONH was measured as a function of distance from the lower optic disc margin by using the software supplied by Heidelberg Engineering (Fig. S3).

Electron Microscopy

The enucleated rabbit eyes were fixed in the same manner as the H&E stain. The eyes were subsequently fixed in 1% osmium tetroxide for 90 min. The retina was dehydrated through a graded series of ethanol (50–100%), cleared in propylene oxide, and embedded in epoxy resin. Ultrathin sections were cut by using an ultramicrotome and stained with uranyl acetate and lead citrate. For ultrastructural immunohistochemistry, the enucleated RP rabbit eyes were fixed in 4% paraformaldehyde and 0.05% glutaraldehyde for 4 h. The fixed retina was cut with a microslicer (Microslicer DTK-1000, Dosaka EM, Kyoto, Japan) into sections with a thickness of 65 μm . The sections were incubated with mouse monoclonal anti-rhodopsin antibody (Ret-P1 (sc-57433), Santa Cruz, California, U.S.A.) and subsequently, with gold-conjugated Fab fragment of goat anti-mouse IgG (Nanogold, Molecular Probes, Inc., Oregon, U.S.A.), followed by silver enhancement (HQ Silver, Nanoprobes, Inc., New York, U.S.A.). The stained sections were observed by transmission electron microscopy (H-7650, Hitachi Co., Tokyo, Japan).

Statistical analysis

Data from WT and RP rabbits were analyzed with an unpaired *t*-test by using PASW Statistics version 18.0 (SPSS Inc., Chicago, IL). The level of statistical significance was set at $P < 0.05$.

Supporting Information

Figure S1 Ultrastructure of photoreceptors in 20-week-old WT and RP rabbits. (A, B) Ultrastructure of photoreceptors in 20-week-old WT rabbits. The inner segments of photoreceptors (IS) and the outer segments of photoreceptors (OS) were regular and dense. (C, D) Ultrastructural changes in 20-week-old RP rabbits. The IS and OS were mostly absent, and the residual IS and OS were less organized than those in WT rabbits. In the magnified image (D), many small vesicles (arrowheads) appeared to be cleaved from the IS into the extracellular space around the photoreceptors (arrows). (TIF)

References

- Hartong DT, Berson EL, Dryja TP (2006) Retinitis pigmentosa. *Lancet* 368: 1795–1809.
- Mendes HF, van der Spuy J, Chapple JP, Cheetham ME (2005) Mechanisms of cell death in rhodopsin retinitis pigmentosa: implications for therapy. *Trends Mol Med* 11: 177–185.
- Peters RM, Alexander CA, Wells KD, Collins EB, Sommer JR, et al. (1997) Genetically engineered large animal model for studying cone photoreceptor survival and degeneration in retinitis pigmentosa. *Nat Biotechnol* 15: 965–970.
- Narfström K (1983) Hereditary progressive retinal atrophy in the Abyssinian cat. *J Hered* 74: 273–276.
- Chader GJ (2002) Animal models in research on retinal degenerations: past progress and future hope. *Vision Res* 42: 393–399.
- Petersen-Jones SM (1998) Animal models of human retinal dystrophies. *Eye (Lond)* 12(Pt 3b): 566–570.
- Barnett KC, Curtis R (1985) Autosomal dominant progressive retinal atrophy in Abyssinian cats. *J Hered* 76: 168–170.
- Menotti-Raymond M, David VA, Schäffer AA, Stephens R, Wells D, et al. (2007) Mutation in CEP290 discovered for cat model of human retinal degeneration. *J Hered* 98: 211–220.
- Kijas JW, Cideciyan AV, Aleman TS, Pianta MJ, Pearce-Kelling SE, et al. (2002) Naturally occurring rhodopsin mutation in the dog causes retinal dysfunction and degeneration mimicking human dominant retinitis pigmentosa. *Proc Natl Acad Sci U S A* 99: 6328–6333.
- Ng YF, Chan HH, Chu PH, To CH, Gilger BC, et al. (2008) Multifocal electroretinogram in rhodopsin P347L transgenic pigs. *Invest Ophthalmol Vis Sci* 49: 2208–2215.
- Famiglietti EV, Sharpe SJ (1995) Regional topography of rod and immunocytochemically characterized “blue” and “green” cone photoreceptors in rabbit retina. *Vis Neurosci* 12: 1151–1175.
- Rockhill RL, Daly FJ, MacNeil MA, Brown SP, Masland RH (2002) The diversity of ganglion cells in a mammalian retina. *J Neurosci* 22: 3831–3843.
- Marc RE (1986) Neurochemical stratification in the inner plexiform layer of the vertebrate retina. *Vision Res* 26: 223–238.
- Vancy DI, Young HM, Gynther IC (1991) The rod circuit in the rabbit retina. *Vis Neurosci* 7: 141–154.
- Osakada F, Hirami Y, Takahashi M (2009) Stem cell biology and cell transplantation therapy in the retina. *Biotechnol Genet Eng Rev* 26: 297–334.
- Stanzel BV, Liu Z, Brinken R, Braun N, Holz FG, et al. (2012) Subretinal delivery of ultrathin rigid-elastic cell carriers using a metallic shooter instrument and biodegradable hydrogel encapsulation. *Invest Ophthalmol Vis Sci* 53: 490–500.
- Acland GM, Aguirre GD, Ray J, Zhang Q, Aleman TS, et al. (2001) Gene therapy restores vision in a canine model of childhood blindness. *Nat Genet* 28: 92–95.
- Tao W, Wen R, Goddard MB, Sherman SD, O'Rourke PJ, et al. (2002) Encapsulated cell-based delivery of CNTF reduces photoreceptor degeneration in animal models of retinitis pigmentosa. *Invest Ophthalmol Vis Sci* 43: 3292–3298.
- Bush RA, Lei B, Tao W, Raz D, Chan CC, et al. (2004) Encapsulated cell-based intraocular delivery of ciliary neurotrophic factor in normal rabbit: dose-dependent effects on ERG and retinal histology. *Invest Ophthalmol Vis Sci* 45: 2420–2430.
- Kondo M, Sakai T, Komcima K, Kurimoto Y, Ueno S, et al. (2009) Generation of a transgenic rabbit model of retinal degeneration. *Invest Ophthalmol Vis Sci* 50: 1371–1377.
- Wojtkowski M, Bajraszewski T, Gorczynska I, Targowski P, Kowalczyk A, et al. (2004) Ophthalmic imaging by spectral optical coherence tomography. *Am J Ophthalmol* 138: 412–419.
- Chen TC, Cense B, Pierce MC, Nassif N, Park BH, et al. (2005) Spectral domain optical coherence tomography: ultra-high speed, ultra-high resolution ophthalmic imaging. *Arch Ophthalmol* 123: 1715–1720.
- Sakamoto A, Hangai M, Yoshimura N (2008) Spectral-domain optical coherence tomography with multiple B-scan averaging for enhanced imaging of retinal diseases. *Ophthalmology* 115: 1071–1078.

Figure S2 Measurement of mean total retinal thickness.

(A) An infrared image on volume scan mode of SD-OCT. In the volume scan mode, the region ventral to the optic disc, including visual streak (19 lines in vertical $15^\circ \times$ horizontal 30°) was imaged. (B) One of the 19 horizontal OCT sections on volume scan mode. The lines of the vitreoretinal interface and the Bruch's membrane are manually delineated at each horizontal section (C). (D) The retinal thickness map constructed from the volume scan OCT images. Total retinal thickness was measured within the red circle shown (E). The diameter of the red circle was 1 mm, and the center was 3 mm ventral to the inferior edge of the ONH (D, E). (TIF)

Figure S3 Measurement of the thickness of individual retinal layers.

Four vertical OCT sections that pass through the center of the ONH and visual streak are shown. On each section, the boundary lines between each retinal layer were manually delineated. The ONL, ELM–BM, INL, and GCC thicknesses were evaluated in 0.5-mm segments as a function of the distance from the inferior optic disc margin up to 4.0 mm ventral to the inferior edge of the ONH. ONL, outer nuclear layer; ELM, external limiting membrane; BM, Bruch's membrane; INL, inner nuclear layer; and GCC, ganglion cell complex. (TIF)

Acknowledgments

We thank Michiko Tsuji, Yuri Terado, and Noriko Suzuki for their technical assistance; Megan Oliver for critical reading of the manuscript; Yuji Nishizawa of Chubu University for his advice on immunohistochemistry; and Gerhald Zinser of Heidelberg Engineering for discussion on the *Multiline* OCT. Presented in part at the Association Research in Vision and Ophthalmology (ARVO) Annual Meeting, May 2011; Florida, U.S.A.

Author Contributions

Conceived and designed the experiments: HOI YM NY. Performed the experiments: YM NN MH MK HT AK. Analyzed the data: YM. Contributed reagents/materials/analysis tools: YT KOF HK. Wrote the paper: YM HOI.

24. Hangai M, Yamamoto M, Sakamoto A, Yoshimura N (2009) Ultrahigh-resolution versus speckle noise-reduction in spectral-domain optical coherence tomography. *Opt Express* 17: 4221–4235.
25. Byeon SH, Chu YK, Lee H, Lee SY, Kwon OW (2009) Foveal ganglion cell layer damage in ischemic diabetic maculopathy: correlation of optical coherence tomographic and anatomic changes. *Ophthalmology* 116: 1949–1959.
26. Nakano N, Hangai M, Nakanishi H, Mori S, Nukada M, et al. (2011) Macular Ganglion Cell Layer Imaging in Preperimetric Glaucoma with Speckle Noise-Reduced Spectral Domain Optical Coherence Tomography. *Ophthalmology* 118: 2414–2426.
27. Sandberg MA, Brockhurst RJ, Gaudio AR, Berson EL (2005) The association between visual acuity and central retinal thickness in retinitis pigmentosa. *Invest Ophthalmol Vis Sci* 46: 3349–3354.
28. Costa RA, Calucci D, Skaf M, Cardillo JA, Castro JC, et al. (2004) Optical coherence tomography 3: Automatic delineation of the outer neural retinal boundary and its influence on retinal thickness measurements. *Invest Ophthalmol Vis Sci* 45: 2399–2406.
29. Chen TC, Cense B, Miller JW, Rubin PA, Deschler DG, et al. (2006) Histologic correlation of in vivo optical coherence tomography images of the human retina. *Am J Ophthalmol* 141: 1165–1168.
30. Oishi A, Hata M, Shimozone M, Mandai M, Nishida A, et al. (2010) The significance of external limiting membrane status for visual acuity in age-related macular degeneration. *Am J Ophthalmol* 150: 27–32.
31. Murakami T, Nishijima K, Sakamoto A, Ota M, Horii T, et al. (2011) Association of pathomorphology, photoreceptor status, and retinal thickness with visual acuity in diabetic retinopathy. *Am J Ophthalmol* 151: 310–317.
32. Huber G, Beck SC, Grimm C, Sahaboglu-Tekgoz A, Paquet-Durand F, et al. (2009) Spectral domain optical coherence tomography in mouse models of retinal degeneration. *Invest Ophthalmol Vis Sci* 50: 5888–5895.
33. Kim KH, Puoris'haag M, Magaluri GN, Umino Y, Cusato K, et al. (2008) Monitoring mouse retinal degeneration with high-resolution spectral-domain optical coherence tomography. *J Vis* 8: 17 1–11.
34. Ruggeri M, Wehbe H, Jiao S, Gregori G, Jockovich ME, et al. (2007) In vivo three-dimensional high-resolution imaging of rodent retina with spectral-domain optical coherence tomography. *Invest Ophthalmol Vis Sci* 48: 1808–1814.
35. Srinivasan VJ, Ko TH, Wojtkowski M, Carvalho M, Clermont A, et al. (2006) Noninvasive volumetric imaging and morphometry of the rodent retina with high-speed, ultrahigh-resolution optical coherence tomography. *Invest Ophthalmol Vis Sci* 47: 5522–5528.
36. Fischer MD, Huber G, Beck SC, Tanimoto N, Muehlfriedel R, et al. (2009) Noninvasive, in vivo assessment of mouse retinal structure using optical coherence tomography. *PLoS ONE* 4: 1–7.
37. Nakano N, Ikeda HO, Hangai M, Muraoka Y, Toda Y, et al. (2011) Longitudinal and Simultaneous Imaging of Retinal Ganglion Cells and Inner Retinal Layers in a Mouse Model of Glaucoma Induced by N-Methyl-D-Aspartate. *Invest Ophthalmol Vis Sci* 52: 8754–8762.
38. Yamauchi Y, Agawa T, Tsukahara R, Kimura K, Yamakawa N, et al. (2011) Correlation between high-resolution optical coherence tomography (OCT) images and histopathology in an iodoacetic acid-induced model of retinal degeneration in rabbits. *Br J Ophthalmol* 95: 1161–1165.
39. Li T, Snyder WK, Olsson JE, Dryja TP (1996) Transgenic mice carrying the dominant rhodopsin mutation P347S: evidence for defective vectorial transport of rhodopsin to the outer segments. *Proc Natl Acad Sci U S A* 93: 14176–14181.
40. Aleman TS, Cideciyan AV, Sumaroka A, Windsor EA, Herrera W, et al. (2008) Retinal laminar architecture in human retinitis pigmentosa caused by Rhodopsin gene mutations. *Invest Ophthalmol Vis Sci* 49: 1580–1590.
41. Milam AH, Li ZY, Fariss RN (1998) Histopathology of the human retina in retinitis pigmentosa. *Prog Retin Eye Res* 17: 175–205.
42. Humayun MS, Prince M, de Juan E, Jr., Barron Y, Moskowitz M, et al. (1999) Morphometric analysis of the extramacular retina from postmortem eyes with retinitis pigmentosa. *Invest Ophthalmol Vis Sci* 40: 143–148.

RESEARCH REPORT

Clinical features of a Japanese case with Bothnia dystrophy

Kazutoshi Nojima¹, Katsuhiko Hosono¹, Yang Zhao^{1,2}, Takaaki Toshiba¹, Akiko Hikoya¹, Tatsuhiko Asai¹, Masaru Kato³, Mineo Kondo⁴, Shinsei Minoshima², and Yoshihiro Hotta¹

¹Department of Ophthalmology, Hamamatsu University School of Medicine, Hamamatsu, Japan, ²Department of Photomedical Genomics, Basic Medical Photonics Laboratory, Medical Photonics Research Center, Hamamatsu University School of Medicine, Hamamatsu, Japan, ³Department of Ophthalmology, Seirei Mikatahara Hospital, Hamamatsu, Japan, and ⁴Department of Ophthalmology, Nagoya University Graduate School of Medicine, Nagoya, Japan

ABSTRACT

Purpose: Bothnia dystrophy is a variant of recessive retinitis punctata albescens (RPA) and is caused by a homozygous R234W mutation in the *RLBP1* gene. We report the clinical features of a Japanese patient with the homozygous R234W mutation in the *RLBP1* gene.

Methods: An affected woman with RPA has been examined clinically for 25 years. Her DNA was obtained with informed consent, and the exons and surrounding areas of *RDH5*, rhodopsin, and *RLBP1* were amplified by PCR and directly sequenced.

Results: Our patient was first examined in our hospital in 1986 when she was 6 years old. Ophthalmoscopy showed numerous small white dots in the posterior pole of both eyes. Although the a- and b-waves of the single flash ERGs were severely reduced after a standard 30 min of dark-adaptation, the amplitudes of both waves increased markedly after 24 hr of dark-adaptation. The visual disturbances and visual field scotomas became more evident in her twenties, and her BCVAs were 0.2 OD and 0.5 OS when she was 31 years old in 2010. Fundus examinations showed macular degeneration in both eyes. A homozygous R234W mutation was detected in *RLBP1*, and no mutations were detected in *RDH5* and rhodopsin.

Conclusions: The clinical characteristics of a Japanese patient with a homozygous R234W mutation in *RLBP1* are very similar to that of Swedish patients with Bothnia dystrophy. The origin of the Japanese R234W mutation is probably not the same as that of the Swedish patients, but more likely due to the high incidence of C to T transitions.

Keywords: Retinitis punctata albescens, Bothnia dystrophy, *RLBP1* gene, *RDH5* gene, electroretinograms

INTRODUCTION

The flecked retina syndrome includes benign (familial) flecked retina, fundus albipunctatus, and retinitis punctata albescens (RPA) (OMIM #136880, 228980). The benign (familial) flecked retina is typically not associated with nyctalopia or a delay in dark-adaptation.¹ Although young patients with fundus albipunctatus and RPA can have similar symptoms and signs, RPA is progressive and associated with a severe decrease in the amplitudes of the electroretinograms (ERGs). The amplitudes do not recover even after prolonged

dark-adaptation. The retinal changes can progress to generalized atrophy of retina.

Mutations in the *RDH5* gene have been found in patients with fundus albipunctatus in various ethnic groups and also in patients with cone dystrophy associated with fundus albipunctatus.^{2–5} A consanguineous Saudi Arabian kindred with a retinal dystrophy phenotype that fulfilled the criteria of fundus albipunctatus in younger individuals and RPA in older patients with the R150Q mutation of *RLBP1* gene has also been reported.⁶ Mutations in the genes encoding rhodopsin (*RHO*), peripherin/RDS (*PRPH2*),

Received 19 June 2011; revised 19 September 2011; accepted 01 October 2011

Correspondence: Yoshihiro Hotta, MD, Department of Ophthalmology, Hamamatsu University School of Medicine, 1-20-1 Handayama, Hamamatsu 431–3192, Japan. Tel: +81 53 435 2256. Fax: +81 53 435 2372. E-mail: hotta@hama-med.ac.jp

and retinaldehyde-binding protein (*RLBP1*) have been reported in patients with RPA,⁷⁻¹² whereas *RLBP1* gene mutations cause autosomal recessive retinitis pigmentosa, RPA, fundus albipunctatus, and Newfoundland rod-cone dystrophy (OMIM# 607476).^{9,13,14}

Bothnia dystrophy (BD, OMIM#607475) is an atypical form of RPA and is caused by an arginine-to-tryptophan missense mutation at position 234, R234W, in the *RLBP1* gene.¹⁵ We report a Japanese case of RPA with a homozygous R234W mutation suggesting a Japanese case of BD. We were able to follow our patient for 25 years and confirmed the significant recovery of the full-field ERGs after 24 hrs of dark-adaptation.

MATERIALS AND METHODS

Patient

A 6-year-old Japanese girl was first examined in our hospital in 1986 because of night blindness which was first noticed at the age of 2 years. She underwent periodic ophthalmological examinations over the next 25 years in the Department of Ophthalmology, Hamamatsu University Hospital, Hamamatsu, Japan. None of the individuals in her family had BD or other ocular diseases. Her father and mother are not relatives but her paternal ancestors were from Shinshiro city and her maternal ancestors from Mikawaichinomiya-cho. These cities are in the Aichi prefecture and are situated close to each other.

The visual acuity (VA) was determined using a decimal visual acuity chart. The visual fields were determined with a Goldmann perimeter using standard targets. The course of dark-adaptation was determined

with a Goldmann-Weekers adaptometer. Color vision was tested with the Ishihara pseudoisochromatic plates (38 plates; 2002 edition) and Panel D-15 test.

Electroretinographic Analyses

Full-field ERGs were elicited with a Ganzfeld dome and recorded with a unipolar contact lens electrode. The reference and ground electrodes were attached to the forehead and the ipsilateral ear, respectively. After 30 min of dark-adaptation, a rod response was elicited by a white flash at an intensity of 0.01cd-s/m⁻². Single-flash cone responses and 30 Hz flicker responses were elicited by white stimuli of 3.0cd-s/m⁻² on a white background of 81cd/m⁻². Maximal rod-cone responses were elicited by a bright white flash (20 Joules) at an intensity of 10.0cd-s/m⁻². The maximal rod-cone responses were also recorded after a prolonged dark-adaptation of 3 hrs and 24 hrs when the patient was 7 and 32 years old.

Mutation Analyses

This study was approved by the Institutional Review Board for Human Genetic and Genome Research of the Hamamatsu University School of Medicine, and procedures were performed in accordance with the Declaration of Helsinki. An informed consent was obtained from the patient. Genomic DNA was extracted from peripheral lymphocytes by standard procedures. Polymerase chain reaction (PCR) was performed using the KOD -Plus-ver.2 (TOYOBO, Japan) with published primers¹⁶ and the primer sets shown in Table 1. PCR was performed according to the manufacturer's protocol at

TABLE 1 PCR primer sequences for *RDH5*, *RHO*, and *RLBP1*

Gene	Exon	PCR primer		PCR product size (bp)
		Forward	Reverse	
<i>RDH5</i> *	2	GGCCACAGTAAACTGGACAA	TTCCTGGTGGTCTACCATAC	405
	3	CCCCAGCATCCTTTTCATCT	GGTCACAAAGCTTACATAAGGGTA	454
	4	AAGAACCCAGCAACTTCGCT	TTCCCTTCATGTGCCCTGT	237
	5	CTGATTGCAACCACCTATGG	CAATCTCTGTGCTGGAAGGCT	276
<i>RHO</i>	1	AATATGATTATGAACACCCCAAT	ACCTAGGACCATGAAGAGGTCAG	460
	1	ACTTCCTCACGCTCTACGTAC	GCACAAACAGCAGCCCGGCTAT	385
	2	TCCTTCCCAAGGCCTCCTCAA	GGTCAGTGCCTGGAACCAGACA	402
	3	AGCCATGCAGACGTTTATGAT	CTTCTGTGTGGTGGCTGACT	454
	4	GTCTTACCGTCAAGGAGGTA	CTGACCCAAGACTGCTGCCAGT	498
	5	CTCAAGCCTCTTGCCCTCCAGT	GGTGGATGTCCCTTCTCAGGCTG	331
<i>RLBP1</i>	3	GCCTCGGGTGATTCTGATGCAAT	ACCCACACAGGGGTTATAGAAG	334
	4	CAGGCTGATGCGGTTGGCTGTT	AGTCTATCAGGTCCAGGATGATCT	302
	5	GCTCTGGCAGGAGACTCATCAC	CCCACAGTATGGAAGCAGGCCT	393
	6	ACTAGGAGGGATGGGGTAGGGAT	GAACCAGGAATGAGGGCCAGT	331
	7	TCCGAGATCAAAGCCTGCAGCAA	AATACTTGGCAAAGTGTCAATCAC	467
	8	GTGATGCTGGACAAGTCTGTTCTA	TAGCTCAGGACCATGGTAGAGTGT	315
	9	ACTGACACCAACATGGAGAC	CAGCCCTTTCCTAGCCTTGGGT	394

**RDH5* primers have been previously described.¹⁶

98°C for 10sec, 60°C for 30sec, and 68°C for 1 min for 35 cycles in an automated thermal cycler (GeneAmp PCR System 9700; Applied Biosystems Foster City, CA, USA). The PCR products were purified with Wizard SV Gel and PCR Clean-up System (Promega, Madison, WI, USA) or treated with Exonuclease I and Antarctic Phosphatase (New England Biolabs, Ipswich, MA, USA). Direct sequencing was performed with the BigDye Terminator v3.1 Cycle Sequencing Kit on an ABI3100 autosequencer (Applied Biosystems, Foster City, CA, USA).

RESULTS

Clinical Findings

At the first visit in 1986 when she was 6 years old, her VA was 1.0 in both eyes without correction, and her refractive errors were +2.50 diopters (D) = -1.25D × 180° in the right eye and +1.50D = -0.50D × 180° in the left eye. The visual fields determined by Goldmann perimeter were full, and the anterior segments determined by slit-lamp microscopic examination were normal (Fig. 1A & B). Ophthalmoscopy showed many small white dots in the posterior pole of both eyes in 1986 and 2003 (Fig. 2A & B, photographs from 2003). She was diagnosed with atypical fundus albipunctatus. The course of both the cone and rod dark-adaptation was abnormal. The color vision determined by the Ishihara chart in 1999 showed that the patient was not able to detect the numbers in 21

plates. The Panel D-15 test performed in 1999 showed color vision defect in both eyes.

The vision disturbances and central scotomas in both eyes were first detected when the patient was in her twenties (Fig. 1C & D).

At 30 years of age, changes in the retinal pigment epithelium (RPE) were observed in both eyes (Fig. 2C & D). Fluorescein angiography was performed in 2010 (Fig. 2E & F), and a diffuse hyperfluorescence was seen in the macular area in the early arteriovenous phase. A granular type hyperfluorescence corresponding to the atrophic area appeared outside the vascular arcades.

Nowadays she is 31 years old and her BCVA is 0.1 OD and 0.5 OS and her refraction are +0.50D = -3.00D × 170° in the right eye and +1.00D = -3.50D × 10° in the left eye.

Optical coherence tomography (OCT) showed a generalized retinal thinning in the central foveal area (Fig. 2G & H).

Electrophysiological Analyses

Representative full-field ERGs are shown in Fig. 3. When the patient was 7 years old, the rod response was undetectable, and the amplitude of the single-flash cone response and 30-Hz flicker response were reduced by about 50% (Fig. 3A). The maximal rod-cone response after 30 min of dark-adaptation was also severely reduced but was still detectable (Fig. 3B, right column). The amplitudes of the ERGs decreased with increasing

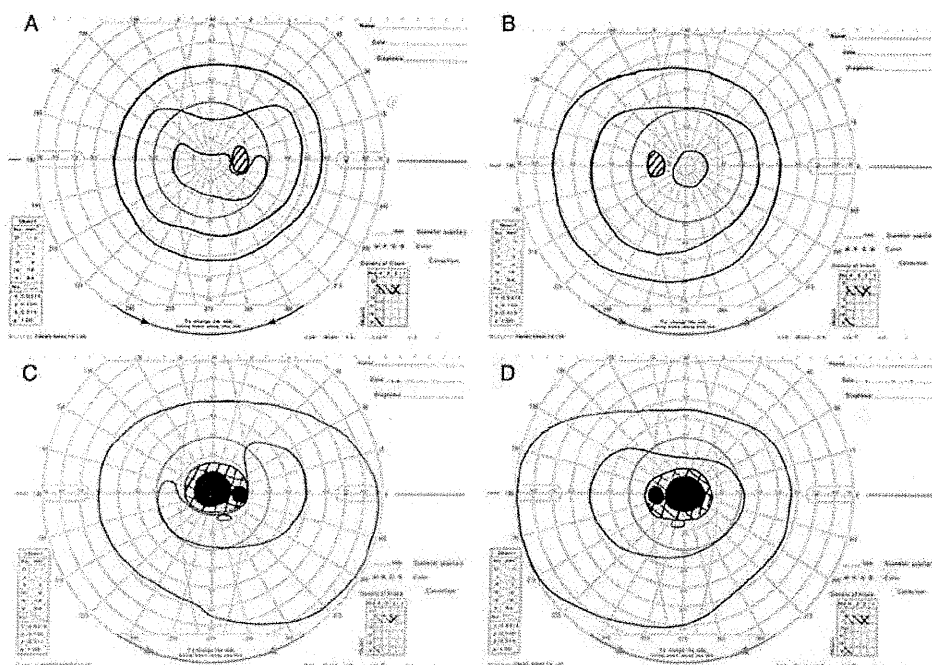


FIGURE 1 Progression of visual field defects in a patient with Bothnia dystrophy. (A and B) Left eye (A) and right eye (B) at age 6 years. Visual fields are essentially normal in both eyes. (C and D) Left eye (C) and right eye (D) at age 30 years. Central scotoma is present in both eyes.

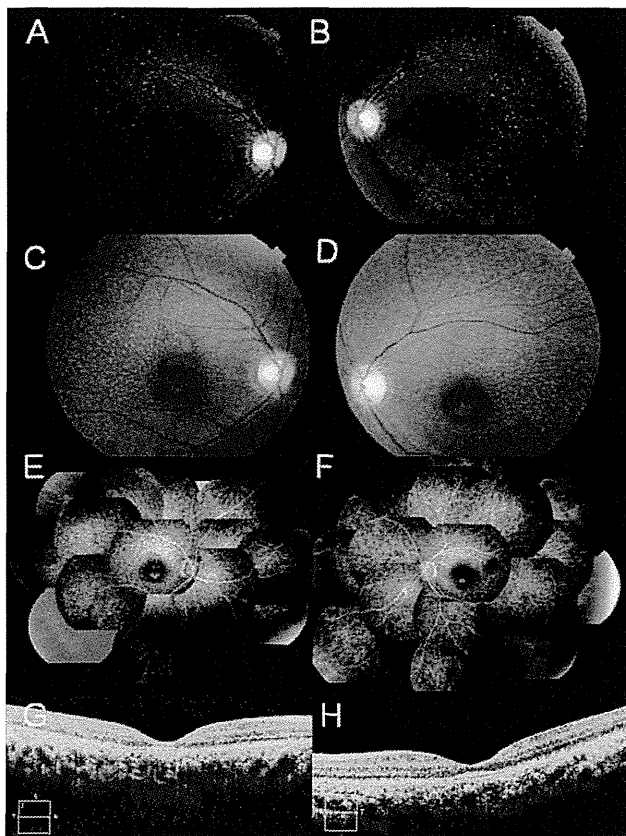


FIGURE 2 Fundus photographs of a patient with Bothnia dystrophy. (A and B) Fundus photograph of the right (A) and left (B) eyes taken at age 23 years. (C and D) Fundus photograph of the right (C) and left (D) eyes taken at age 30 years. Numerous tiny white dots can be seen in both eyes. Changes in the RPE can be seen at age 30 years old in both eyes. (E and F) Fluorescein angiograms of the right eye (E) and left eye (F) taken at age 30 years. The early arteriovenous phase shows a diffuse hyperfluorescence in the macular area. (G and H) Right Cross sectional optical coherence tomographic images of the right (G) and left (H) eyes taken at age 31 years. Retinal thinning can be seen.

age and were almost undetectable when she was 32 years old.

To examine whether these reduced ERG responses were due to a delay of dark-adaptation we recorded the maximal rod-cone ERGs after prolonged dark-adaptation. The amplitude of maximal rod-cone ERG did not increase after 3 hrs dark-adaptation (Fig. 3C, upper trace), but increased by approximately three fold after 24 hrs of dark-adaptation (Fig. 3C, middle trace) when she was 7 years old. This phenomenon was also confirmed when she was 32 years old. The nearly undetectable maximal rod-cone ERG became clearly detectable at 95 μ V after 24 hrs of dark-adaptation (Fig. 3C, lower trace).

Mutation Analyses

Although no mutation was detected in the *RDH5* and rhodopsin genes, a homozygous R234W mutation was detected in the *RLBP1* gene (data not shown).

DISCUSSION

We initially diagnosed our patient with an atypical variant of fundus albipunctatus instead of RPA because the mixed rod-cone response recovered significantly after 24 hrs of dark-adaptation. But the visual disturbances and visual field scotomas appeared in her twenties. At that age, the BCVA was also depressed. Recent investigations of patients with fundus albipunctatus caused by a *RDH5* gene mutation showed that the retinal changes were not stationary and frequently progressed to cone dystrophy in their fifties.¹⁷ Genetic analyses showed a *RLBP1* gene mutation instead of a *RDH5* gene mutation confirming our diagnosis of RPA.

RLBP1 gene mutations cause autosomal recessive retinitis pigmentosa (RP), RPA, fundus albipunctatus, and Newfoundland rod-cone dystrophy.^{9,13,14} Known allelic variants of the *RLBP1* gene now include missense mutations, frameshift mutations that result in truncation, and canonical splice donor site mutations that prevent translation of the protein. Our case is the second report of a *RLBP1* mutation in a Japanese patient with the RPA phenotype. The number of patients with RPA seems to be fewer than those with fundus albipunctatus in Japan. The other Japanese case with the *RLBP1* mutation was due to compound heterozygous mutations of R103W and R234W and had the RPA phenotype.¹⁸

The atypical variant of autosomal recessive retinitis pigmentosa (RP) was known to clinicians in northern Sweden for decades as Västerbotten dystrophy or BD and has been well characterized.^{19–21} BD patients have night blindness from early childhood, followed by macular degeneration and a decrease in visual acuity that lead to legal blindness in early adulthood. The disorder has been associated with a missense mutation, R234W, in the *RLBP1* gene. Because we detected a homozygous R234W mutation, this is the first non-Swedish patient with BD if the gene mutation determined the disease nomenclature. To support this, our case had the typical clinical features described for BD patients.

Although the parents of our case are not relatives, consanguinity might be suspected because her parent's ancestors lived in adjacent areas. In 1999, Morimura⁹ reported that a patient who was a member of Swedish pedigree had a homozygous R234W mutation. Because the R234W mutation is not widespread in the world, we suggest that this R234W mutation most likely represents a recurrent mutation rather than a founder mutation of Swedish origin. The R234W mutation is caused by single base substitution from CCG to TGG. Methylated CpG sequences frequently undergo mutation resulting in single base substitution because deamination of 5-methylcytosines easily forms thymine. This conversion of a DNA base from cytosine to thymine within the coding regions can result in a pathogenic mutation. In human genetic diseases, methylated CpG sequences are mutational hotspots.²² Thus, the Japanese R234W

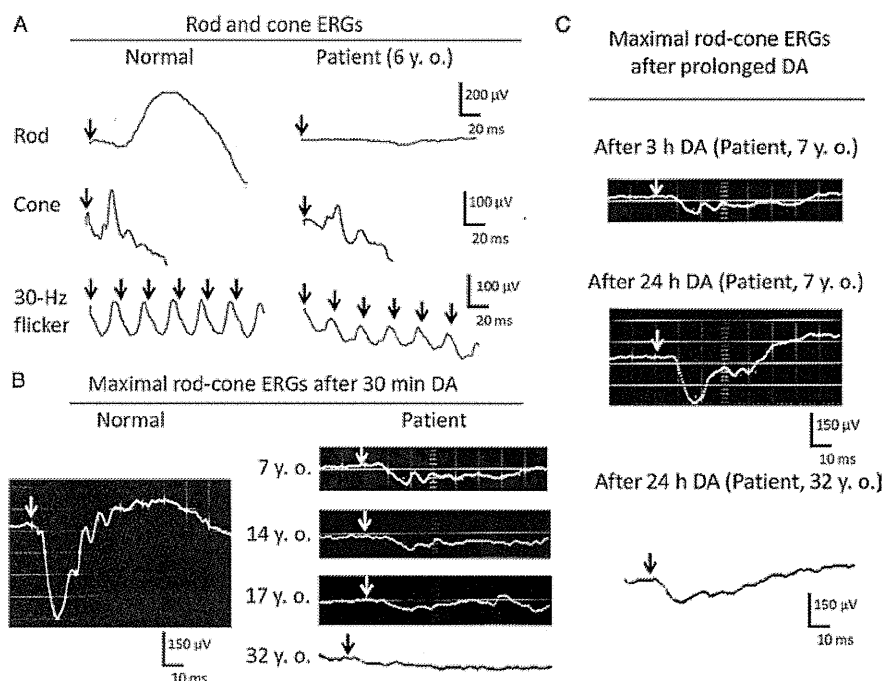


FIGURE 3 Full-field electroretinograms (ERGs) recorded from a patient with Bothnia dystrophy. (A) Rod and cone ERGs recorded from a normal subject (left) and our patient at age 6 years. Arrowheads indicate the onset of the flash stimulus. Rod responses, single-flash cone responses, and 30-Hz flicker ERGs are shown. (B) Maximal rod-cone ERGs recorded after 30 min of dark-adaptation from a normal subject (left) and our patient at ages 7, 14, 17, and 32 years (right). The ERG amplitudes of our patient decrease with increasing age. (C) Maximal rod-cone ERG responses recorded from our patient after different durations of dark-adaptation. Maximal rod-cone ERG after 3 hrs of dark-adaptation (upper trace) and after 24-hr dark-adaptation (middle trace) when the patient was 7 years old. Maximal rod-cone ERG after 24-hr dark-adaptation recorded from our patient when she was 32 years old (lower trace).

mutation may have occurred at the methylated CpG sequence. Three of the four *RLBP1* gene mutated alleles in Japanese RPA patients are R234W. We could not determine if the R234W mutation in those Japanese RPA patients has a founder effect from a Japanese ancestor or occurred independently. A linkage analysis study on the *RLBP1* locus haplotypes from those patients will be performed in the future to clarify the possibility of a common ancestor.

ACKNOWLEDGMENTS

This study was supported by research grants from the Ministry of Health, Labour and Welfare (Research on Measures for Intractable Diseases) and from Japan Society for the Promotion of Science (Grant-in-Aid for Scientific Research (C) 23592561 and Grant-in Aid for Young Scientists (B) 23791975).

Declaration of interest: The authors report no conflicts of interest. The authors alone are responsible for the content and writing of the paper.

REFERENCES

- Sabel Aish SF, Dajani B. Benign familial fleck retina. *Br J Ophthalmol* 1980;64:652–659.
- Yamamoto H, Simon A, Eriksson U, et al. Mutations in the gene encoding 11-cis retinol dehydrogenase cause delayed dark adaptation and fundus albipunctatus. *Nat Genet* 1999;22:188–191.
- Nakamura M, Hotta Y, Tanikawa A, et al. A high association with cone dystrophy in fundus albipunctatus caused by mutations of the *RDH5* gene. *Invest Ophthalmol Vis Sci* 2000;41:3925–3932.
- Driessen CA, Janssen BP, Winkens HJ, et al. Null mutation in the human 11-cis retinol dehydrogenase gene associated with fundus albipunctatus. *Ophthalmology* 2001;108:1479–1484.
- Hotta K, Nakamura M, Kondo M, et al. Macular dystrophy in a Japanese family with fundus albipunctatus. *Am J Ophthalmol* 2003;135:917–919.
- Katsanis N, Shroyer NF, Lewis RA, et al. Fundus albipunctatus and retinitis punctata albescens in a pedigree with an R150Q mutation in *RLBP1*. *Clin Genet* 2001;59:424–429.
- Kajiwara K, Sandberg MA, Berson EL, et al. A null mutation in the human peripherin/RDS gene in a family with autosomal dominant retinitis punctata albescens. *Nat Genet* 1993;3:208–212.
- Souied E, Soubrane G, Benlian P, et al. Retinitis punctata albescens associated with the Arg135Trp mutation in the rhodopsin gene. *Am J Ophthalmol* 1996;121:19–25.
- Morimura H, Berson EL, Dryja TP. Recessive mutations in the *RLBP1* gene encoding protein in a form of retinitis punctata albescens. *Invest Ophthalmol Vis Sci* 1999;40:1000–1004.
- Fishman GA, Roberts MF, Derlacki DJ, et al. Novel mutations in the cellular retinaldehyde-binding protein gene (*RPBP1*) associated with retinitis punctata albescens. *Arch Ophthalmol* 2004;122:70–75.
- Humbert G, Delettre C, Sénéchal A, et al. Homozygous deletion related to Alu repeats in *RLBP1* causes retinitis punctata albescens. *Invest Ophthalmol Vis Sci* 2006;47:4719–4724.

12. Singh HP, Jalali S, Narayanan R, et al. Genetic analysis of Indian families with autosomal recessive retinitis pigmentosa by homozygosity screening. *Invest Ophthalmol Vis Sci* 2009;50:4065–4071.
13. Maw MA, Kennedy B, Knight A, et al. Mutation of the gene encoding cellular retinaldehyde-binding protein in autosomal recessive retinitis pigmentosa. *Nat Genet* 1997;17:198–200.
14. Eichers ER, Green JS, Stockton DW, et al. Newfoundland rod-cone dystrophy, an early-onset retinal dystrophy, is caused by splice-junction mutation in *RLBP1*. *Am J Hum Genet* 2002;70:955–964.
15. Burstedt MS, Sandgren O, Holmgren G, et al. Bothnia dystrophy caused by mutations in the cellular retinaldehyde-binding protein gene (*RLBP1*) on chromosome 15q26. *Invest Ophthalmol Vis Sci* 1999;40:995–1000.
16. Wang C, Nakanishi N, Ohishi K, et al. Novel *RDH5* mutation in family with mother having fundus albipunctatus and three children with retinitis pigmentosa. *Ophthalmic Genet* 2008;29:29–32.
17. Nakamura M, Skalet J, Miyake Y. *RDH5* gene mutations and electroretinogram in fundus albipunctatus with or without macular dystrophy. *Doc Ophthalmol* 2003;107:3–11.
18. Nakamura M, Lin J, Ito Y, et al. Novel mutation in *RLBP1* gene in a Japanese patient with retinitis punctata albescens. *Am J Ophthalmol* 2005;139:1133–1135.
19. Burstedt MS, Forsmann-Semb K, Golovleva I, et al. Ocular phenotype of Bothnia dystrophy, an autosomal recessive retinitis pigmentosa associated with an R234W mutation in the *RLBP1* gene. *Arch Ophthalmol* 2001;119:260–267.
20. Burstedt MS, Sandgren O, Golovleva I. Effect of prolonged dark adaptation in patients with retinitis pigmentosa of Bothnia type: an electrophysiological study. *Doc Ophthalmol* 2008;116:193–205.
21. Burstedt MS, Golovleva I. Central retinal finding in Bothnia dystrophy caused by *RLBP1* sequence variation. *Arch Ophthalmol* 2010;128:989–995.
22. Sved J, Bird A. The expected equilibrium of the CpG dinucleotide in vertebrate genomes under a mutation model. *Proc Natl Acad USA* 1990;87:4692–4696.

Toppan Best-set Premedia Limited		
Journal Code: CXO		Proofreader: Elsie
Article No: CXO796		Delivery date: 30 Jul 2012
Page Extent: 6		

CLINICAL AND EXPERIMENTAL

OPTOMETRY

RESEARCH PAPER

Low luminance visual acuity in patients with central serous chorioretinopathy

Clin Exp Optom 2012

DOI:10.1111/j.1444-0938.2012.00796.x

Kyoko Fujita* MD PhD
Kei Shinoda† MD PhD
Celso Soiti Matsumoto¹ MD PhD
Yutaka Imamura[§] MD PhD
Yoshihiro Mizutani* MD, PhD
Etsuko Tanaka^{||} PhD
Atsushi Mizota[†] MD, PhD
Koichi Oda[†] PhD
Mitsuko Yuzawa* MD PhD
* Department of Ophthalmology, Surugadai Nihon University Hospital, Tokyo, Japan
† Department of Ophthalmology, Teikyo University School of Medicine, University Hospital Itabashi, Tokyo, Japan
§ Department of Ophthalmology, Teikyo University School of Medicine, University Hospital Mizonokuchi, Kanagawa, Japan
|| Department of Ophthalmology, Kyorin University School of Medicine, Tokyo, Japan
† Department of Communication, Tokyo Women's Christian University, Tokyo, Japan
E-mail: shinodak@med.teikyo-u.ac.jp

Submitted: 25 January 2012
Revised: 25 May 2012 Accepted for publication: 4 June 2012

Background: The aim was to determine the low luminance visual acuity in eyes with central serous chorioretinopathy.

Methods: Seven eyes of seven patients with central serous chorioretinopathy and six eyes of six age-matched normal volunteers were examined. Low luminance visual acuity charts were created by an Apple Power Mac G5 computer and displayed on a cathode ray tube monitor (SONY GDM-F500). The background luminance was set at six different levels from 78.20 cd/m² to 0.37 cd/m². The visual acuities of the eyes with central serous chorioretinopathy at each of the six luminance levels were compared to those from their fellow eyes and to normal eyes.

Results: The mean visual acuities varied from 0.13, 0.23, 0.29, 0.42, 0.62 to 0.70 logMAR units as luminance varied from high to low. At the lowest luminance (0.37 cd/m²), five of the seven eyes could not read any character. The mean visual acuities of the fellow eyes at the same luminance levels were 0.03, 0.06, 0.11, 0.20, 0.27 and 0.45 logMAR units and those of the normal volunteers were 0, 0.03, 0.08, 0.14, 0.23 and 0.38 logMAR units, respectively. The visual acuities of the eyes with central serous chorioretinopathy were significantly poorer than those of the normal eyes at all luminance levels except 0.37 cd/m² ($p < 0.05$ for all).

Conclusions: Although the eyes from all three groups had 0 logMAR units visual acuity under standard testing condition, the visual acuity of the eyes with central serous chorioretinopathy were significantly worse at low luminance levels. The low luminance visual acuity may provide information on the visual disturbances reported by central serous chorioretinopathy patients with 0 logMAR units visual acuity.

Key words: central serous chorioretinopathy, contrast sensitivity, low luminance visual acuity, optical coherence tomography, serous retinal detachment

Central serous chorioretinopathy (CSC) is characterised by a serous retinal detachment in the macular area. Central serous chorioretinopathy patients range in age from 20 to 50 years but most are middle-aged men. The central serous chorioretin-

opathy causes a central and paracentral relative scotoma in the visual field.¹⁻³ Although the visual acuity (VA) is relatively good, patients often complain of difficulty with visual activities performed in the evening and at night under low

ambient illumination. In conventional VA tests, such visual disturbances are usually not detected because the backgrounds of VA testing charts have high luminance.

To evaluate patients with central serous chorioretinopathy and visual disturbances